Synthesis and Study of Dielectric and Magnetic Properties of Transition Metals Doped Barium Hexaferrite

By

Hadiqa Kayani

School of Chemical and Materials Engineering

National University of Sciences and Technology

2020

Synthesis and Study of Dielectric and Magnetic Properties of Transition Metals Doped Barium Hexaferrite

Name: Hadiqa Kayani

Registration No: Fall 2018-NSE 06, 00000273644

This thesis is submitted as a partial fulfillment of the requirements for the degree of

Master of Science in Nanoscience and Engineering

Supervisor Name: Dr. Iftikhar Hussain Gul

School of Chemical and Materials Engineering (SCME)

National University of Sciences and Technology (NUST)

H-12 Islamabad, Pakistan

2020

Dedication

I dedicate this thesis to my family; the symbol of love and giving, my father Tahir Mahmood Kayani, my mother Robina kausar and my siblings, my friends, who encourage and support me and my supervisor, who has been a constant source of knowledge and inspiration. I couldn't be able to achieve this milestone without them. This work is sign of my love to them.

Acknowledgements

‘‘Praise is to the One, the Almighty, the merciful and the beneficent Allah, who is the source of all knowledge and wisdom, taught us what we knew not’’.

We offer our humblest thank to the holy Prophet (Peace be upon him) who is forever a model of guidance and knowledge for humanity.

It is my privileged to express appreciation and gratitude to my research supervisor Dr. Iftikhar Hussain Gul and my committee members Dr. Zakir Hussain and Dr. Aftab Akram for their constant support, advice, valuable comments and efficient supervision at every stage of research work. Without their support, this could not have been possible.

I acknowledge Dr. Zakir Hussain (Principal, SCME), all faculty members, lab engineers, lab technical staff and non-teaching staff.

I am also grateful to my family, all my friends and colleagues for giving me encouragement, appreciation and help in completing this project.

Sincerely,
Hadiqa Kayani

Abstract

The exceptionally unique magnetic and electric properties of ferrites have always been of strong interest leading to their extensive commercial use. Barium hexaferrite, is one of the materials being used in microwave, electronic and magnetic devices. In present research study, manganese, cobalt and nickel substitution is performed in a series of $BaFe_{12-3x}(MnNiCo)_xO_{19}$ (x= 0, 0.2, 0.35, 0.5). Synthesis was performed using sol gel method and aqueous solutions of nitrates were used to prepare pure and doped barium hexaferrite nanoparticles. Calcination of the prepared samples was performed at 950 ^oC for 5 hours. The samples were characterized using X-ray Diffraction (XRD) and Fourier transform Infrared spectroscopy (FTIR). Impedance analyzer was used to analyze the dielectric properties. Magnetic properties of the samples were studied using Vibrating Sample Magnetometer (VSM). XRD analysis confirms the hexagonal crystal structure of prepared $BaFe_{12-3x}(MnNiCo)_xO_{19}$. Crystallite size was calculated using Debye Scherer formula and it came out in the range of 36 nm-55 nm. Vibrating band positions were studied using FTIR. Dielectric studies revealed an increase in dielectric constant from 2.29×10^2 to 1.45×10^3 at 500 Hz with the increasing dopant concentration. Similarly, with increasing x value, the dielectric loss value was also increased. Magnetic properties of the prepared samples showed an increase in magnetic saturation from 56 emu/g at x = 0 to 60 emu/g at x = 0.5. A decrease in magnetic coercivity has been observed with increasing dopant concentration. The prepared samples showed an enhancement in dielectric and magnetic properties proving to be an efficient candidate for many magnetic and electrical applications.

Table of Contents

List of Figures

List of Tables

List of Abbreviations

Acronym	Meaning
Br	Barium
NPs	Nanoparticles
NCs	Nanocomposite
BaM	Barium Hexaferrite
Mn	Manganese
Ni	Nickel
Co	Cobalt
Fe	Iron
XRD	X-Ray-diffraction
FTIR	Fourier Transform Infrared
VSM	Vibrating sample Magnetometer

Chapter 1

Introduction

Ferrites have always been of strong interest owing to their distinct electrical and magnetic properties. Ferrites, also known as ceramic powders, are non-conductive, hard, brittle and are generally related to the class of mixed oxides of iron in which iron is usually substituted with rare earth elements like Barium and Strontium, and some metallic elements like Cobalt, Nickel, Manganese, Magnesium and copper. Ferrites are most commonly employed in permanent magnets, transformers, microwave devices, data storage devices, magnetic resonance imaging (MRI), and magnetic recording media. Magnetic behavior of ferrites depends on composition as well as on microstructure including pore size distribution, grain boundaries and total porosity. Depending upon the magnetic coercivity, ferrites can be classified as "Soft" and "Hard".

Table 1.1 Soft and Hard Ferrites

Sr No.	Soft Ferrites	Hard Ferrites
1	Have low hysteresis loss.	Have High hysteresis loss.
2	Movement of domain wall is easier.	Movement of domain wall is relatively difficult.
3	Low magnetic coercivity and retentivity values.	High magnetic coercivity and retentivity values.
4	Magnetization and demagnetization are easier.	Difficult to magnetized and demagnetized.
5	Magneto static energy is small.	Magneto static energy is large.
6	Have large permeability and susceptibility values.	Have small permeability and susceptibility values.
7	**Application:** Use to make Electromagnets.	**Application:** Use to make permanent magnetic.
8	**Example:** Ferrites, Garnets, iron silicon alloys.	**Example:** Alnico, Chromium, tungsten, steel, copper nickel iron alloys etc.

1.2 Types of Magnetism

It is evident that orientation of dipoles changes upon interaction with external magnetic field. So, we can classify the magnetic materials based on orientation of their magnetic dipoles relative to each other. Different types of magnetic materials are discussed below:

1.2.1 Diamagnetism

Electrons move around an atom in orbitals and when magnetic field is applied, this orbital motion of electron give rise to diamagnetism. This orbital motion is responsible for the generation of magnetic field which opposes the applied magnetic field. Therefore, the net magnetic moment of an atom is zero in case of diamagnetic materials. As soon as the magnetic field is removed, magnetization in these materials again drops down to zero because thermal intrinsic energy is higher than the potential energy which aligns the dipole and dipole moments tend to randomize due to thermal agitation. [1]

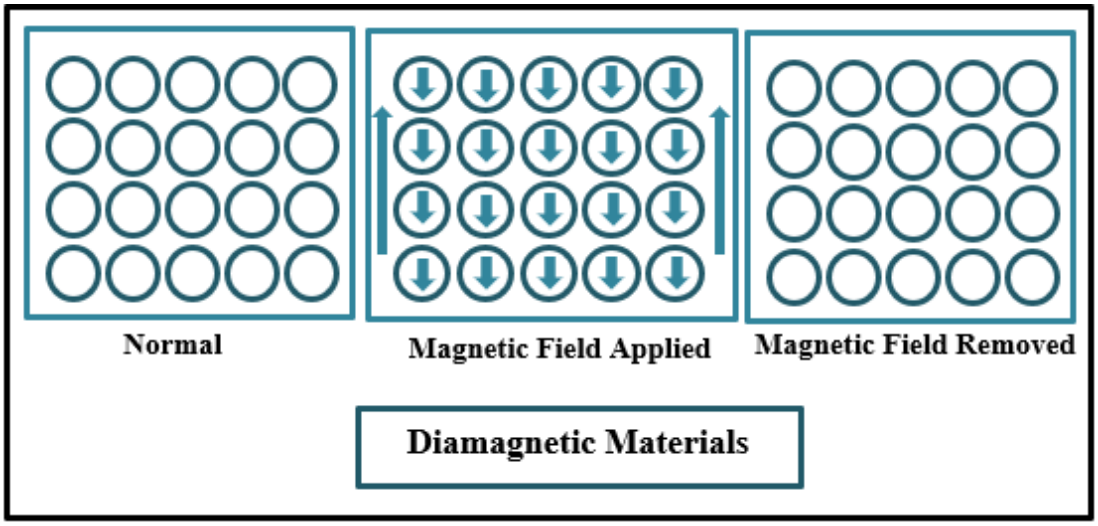

Fig 1.1: Arrangement of Dipoles in Diamagnetic Materials

1.2.2 Para-magnetism

In paramagnetic materials, magnetic dipole moment, associated with few atoms, ions or molecules present in the solid, is permanent. In the absence of magnetic field, net magnetic moment associated with each atom is zero. In the presence of applied

magnetic field, alignment of dipole occurs in the direction of applied field, hence the magnetic susceptibility become positive; $\chi_m > 0$. [2]

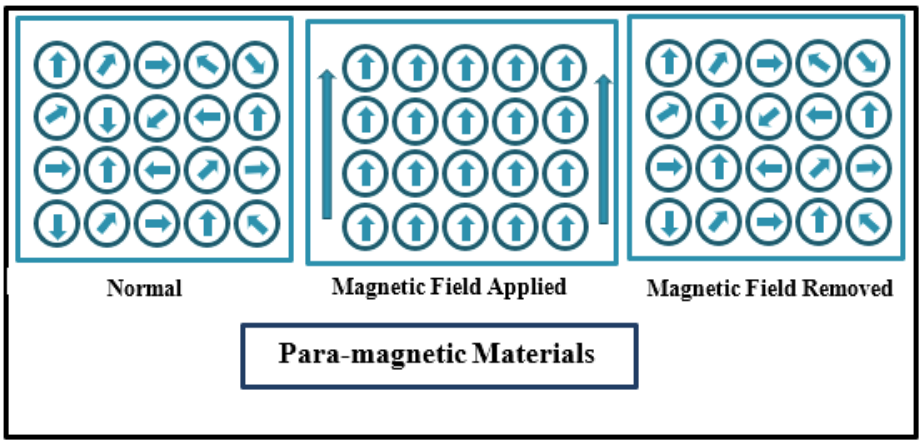

Figure 1.2: Alignment of Dipoles in Paramagnetic Materials

1.2.3 Ferromagnetism

In Ferromagnetic materials, movement of electron pairs in atomic or molecular orbitals results in formation of magnetic dipoles, which spontaneously align parallel to each other causing the phenomena of ferromagnetism. In the absence of magnetic field, the net magnetic moment is still large because of the alignment of dipole in the solid material. Materials having partially filled valence bands/shells usually exhibit this phenomenon and form permanent magnets. Dipoles are aligned in domains and these domains are aligned opposite to each other in bulk of a material resulting in zero net magnetic moment throughout the material. [3]

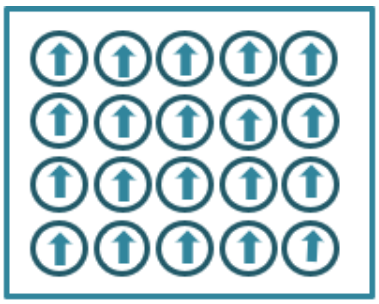

Figure 1.3: Arrangement of Dipoles in Ferromagnetic Materials

1.2.4 Ferrimagnetism

Ferrimagnetism is form of permanent magnetization shown by some of ceramic materials. In ferrimagnetic materials, cations, occupying different crystallographic sites, experience antiferromagnetic coupling and the magnetization of two sublattices is opposite to each other. But net magnetization is non-zero because of unequal strength of the two magnetizations. [4]

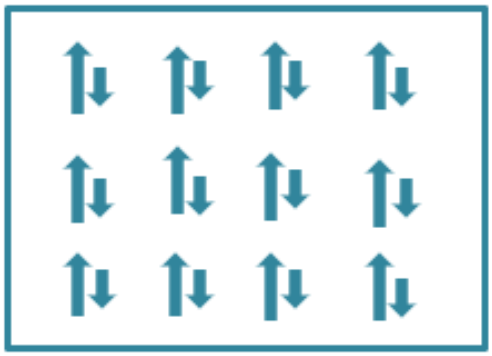

Figure 1.4: Arrangement of Dipoles in Ferrimagnetic Materials

1.2.5 Antiferromagnetism

Anti-ferromagnetism is a phenomenon in which two dipoles arrange themselves in opposite or antiparallel direction. The net magnetization is zero because magnitude of all dipoles is equal. This antiparallel arrangement occurs at a critical temperature called Neel's temperature at which magnetic susceptibility has a maximum value and after this temperature magnetic susceptibility decreases.

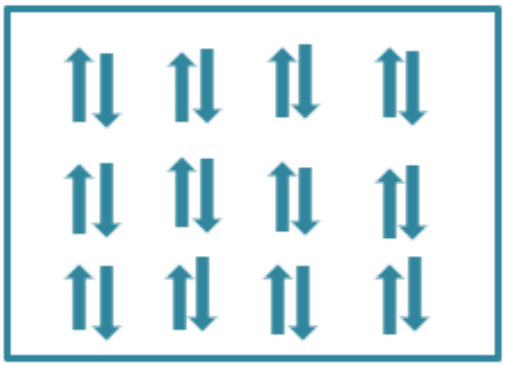

Figure 1.5: Arrangement of Dipoles in Anti-Ferromagnetic Materials

1.3 Classification of Ferrites

The dominant compound in ferrites is Fe_2O_3. So, ferrites are classified on the basis of this compound:

- Spinel Ferrites (Cubic)
- Garnet
- Ortho Ferrites
- Hexaferrites

The molar ratio of Fe_2O_3 to other oxide components in these ceramic compounds help to identify different classes of ferrites as shown the table 1.2:

Table 1.2: Classification of ferrites, (Hench and West 1990)

Type	**Molar Ratio**	**Representation**
Spinel	Fe_2O_3.MeO	MeO represents Transition Metal Oxide
Garnet	$5Fe_2O_3.3Me_2O_3$	Me_2O_3 represents rare earth metal oxides.
Ortho	$AFeO_3$	A represents rare earth metal like HO, Dy, Er, Yb, Y
Hexaferrite	$6Fe_3O_4$.1MeO	MeO represents a Divalent metal oxide from group IIA. For example, BaO, CaO, SrO

1.3.1 Spinel Ferrites

AB_2O_4 represents the crystal structure of spinel ferrite where A and B represents divalent and trivalent cations respectively. Examples of divalent cation include Co^{2+} Ni^{2+} Zn^{+2} Mn^{+2}, Mg^{+2} and trivalent cation can be iron or aluminum etc. Crystal structure of spinel ferrite is acquired from $MgAl_2O_4$, a mineral spinel. Unit cell structure of these spinel ferrites is cubical, and each unit cell contains eight smaller unit cells which are called octanes or formula units. Each unit cell is comprising of 32 oxygen atoms, forming a lattice which is face centered cubic in structure with tetrahedral and octahedral sites. Tetrahedral sites are denoted by A sites and they are surrounded by four oxygen atoms while six oxygen atoms surround the octahedral

sites, represented as B sites. The spinel ferrite structure is not electrically neutral because when metal ions of valency of either +2 or +3 are filled in A and B sites, positive charge dominates. [5]

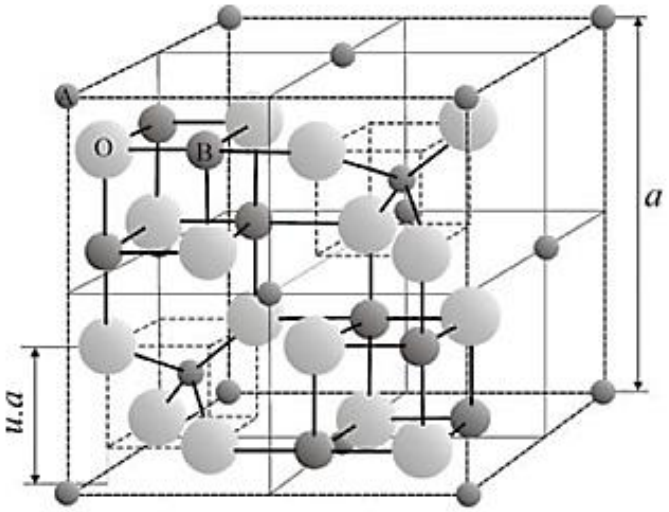

Figure 1.6: Face centered Cubic unit cell of Spinel structure with four formula units: Tetrahedral-A sites are represented by small sphere; Larger spheres represent the Octahedral B site and Oxygen atoms are represented by largest spheres.

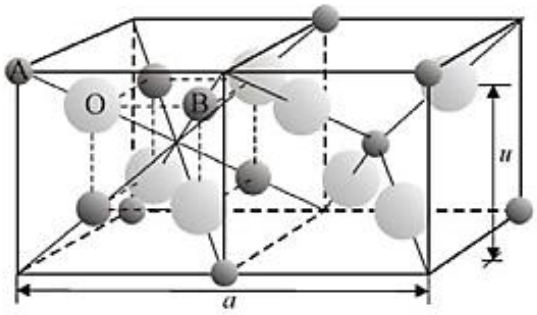

Figure 1.7: Two Adjacent Formula Units of Spinel Structure

1.3.2. Garnets

Garnets are the second group of ferrites with general formula $Me_3B_5O_{12}$ where A represents a rare earth metal cation like yttrium where B represents iron. The unit cell of garnet ferrites is cubical, and it contains eight smaller formula units. In garnet ferrites are comprised of ; Tetrahedral A sites, Octahedral B sites and Dodecahedral C sites. A and B sites have distribution of iron cations (Fe^{3+}) in the ratio of 3:2 while dodecahedral C sites are occupied by Me cations, surrounded by the oxygen atoms [6]. Garnet is known for their optical transparency and for their magneto-optical applications.

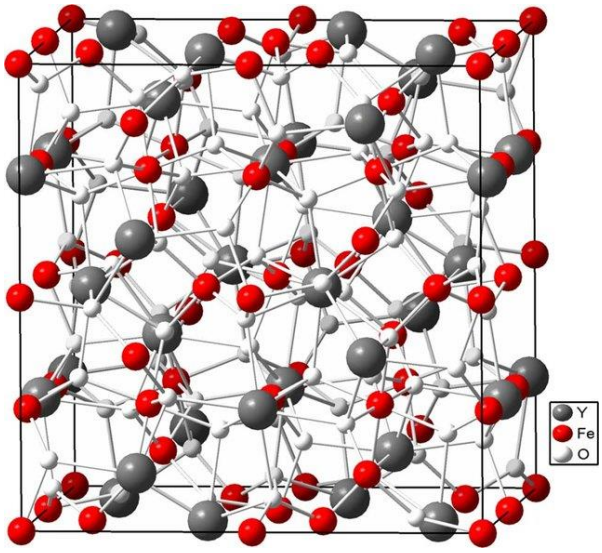

Figure 1.8: Representation of Yttrium and Iron Garnet (YIG) [7]

1.3.3 Ortho Ferrites:

Orthoferrites are third group of ferrites with distorted perovskite structure having a general formula of ABX3 where A is a rare earth or alkaline metal cation, B belongs to transition metal cation usually Iron and X is anionic specie, which is oxygen, in most cases. In orthoferrites, an octahedra is formed by Fe, being the central ion and coordinated by six oxygen atoms. The interstitial sites in octahedral structure are filled by the A cations coordinated by 12 oxygen atoms. Ortho ferrites are known for their high domain wall velocities and have applications in magnetic field sensors, communication technique and electronic current etc. [8]

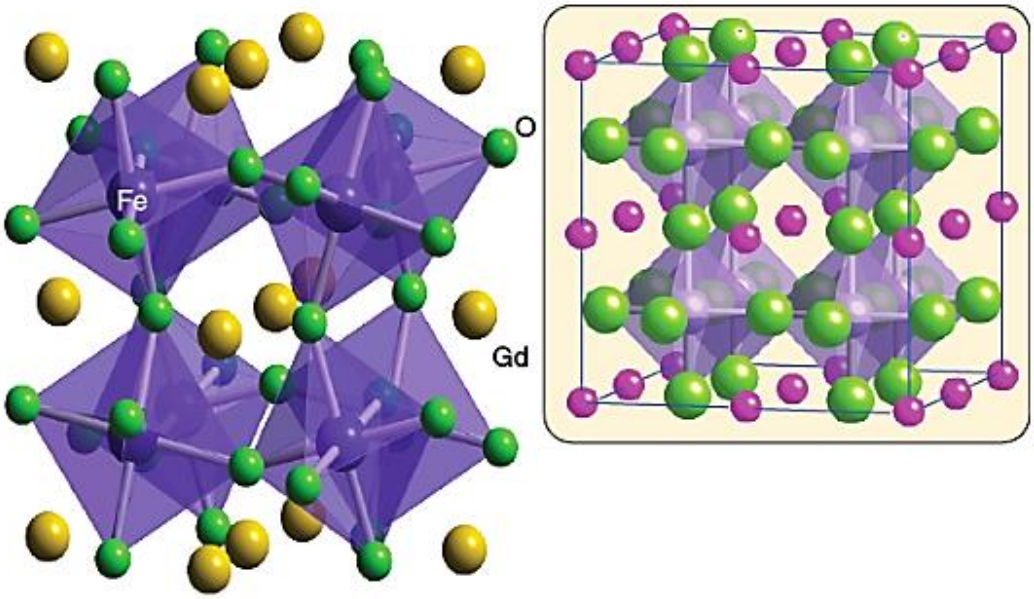

Figure 1.9: Gadolinium Ortho Ferrite

1.3.4 Hexagonal ferrites:

Hexaferrites were first discovered in 1950's and developed over past several decades. Hexaferrites based on barium, strontium and calcium along with iron possess high coercivity and permeability values and can conduct magnetic flux well. This polycrystalline ferrite gained considerable attention in electronic industry because of low cost, easy manufacturing and remarkable electric and magnetic properties.

Hexa-ferrites belong to fourth group of ferrites having hexagonal structure and they are further divided in to six classes named as: M, U, W, X, Y and Z. A large number of hexaferrites can be prepared using different compositions with contrasting magnetic properties [9].

1.3.4.1 Crystal Structure and Composition

Hexaferrites obey the formula $MO+MeO/Fe_2O_3$ where M corresponds to the metals like barium, strontium, calcium etc. whereas Me represents transition metal cation like iron, cobalt, manganese etc. There is a close packing of Oxygen ions layer in the crystal structure of hexaferrite and any divalent of trivalent metal cation reside in the interstices of the structure. Substitution of heavy metal ions like Ba or Sr occur in the

oxygen layers. In hexaferrites, there are essentially 3 fundamental structural blocks names as: S, R and T and they have a rotational symmetry at 180^{o} around the hexagonal c axis represented as S*, R* and T* respectively.

A neutral (RS) block with the total composition of $MFe_{12}O_{19}$ (M Phase) is formed when R subunit combines with S^{+2}. Similarly, a neutral TS can be formed when T subunit combines with S0 with total composition of $Ba_2Me_2Fe_{12}O_{22}$, called as Y phase. Likewise, different composition like X, Y, Z, W, and U can be formed by varying the stacking sequences of hexagonal and cubic units [9].

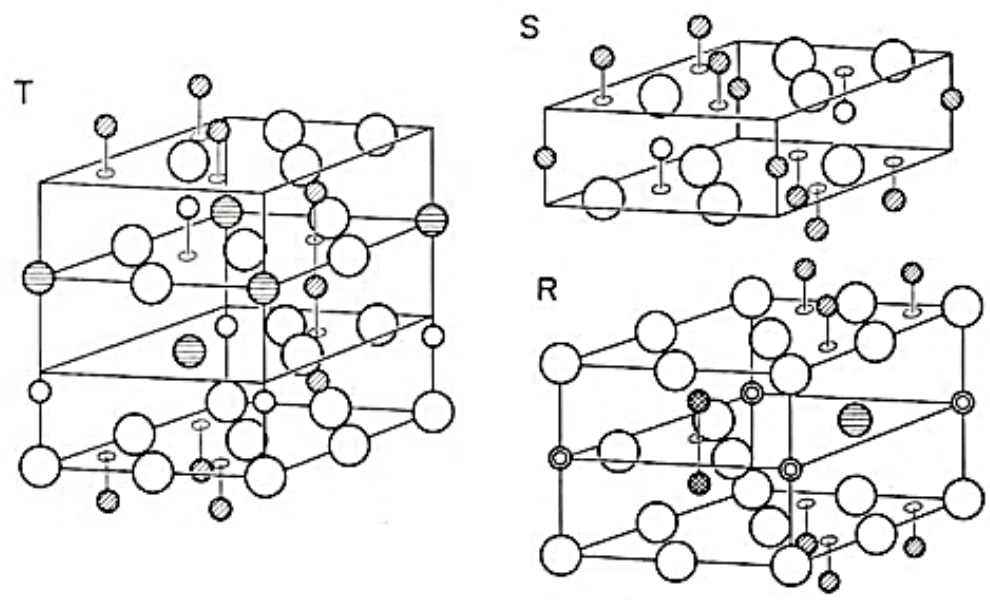

Figure 1.10: Representation of Fundamental blocks S, R and T in Hexaferrites

1.4 M Type Barium Hexaferrite

M-type Barium Hexaferrite, a most commonly produced magnetic material globally, have a melting point of 1390^{o}C with magnetic coercivity of 160-255kAm-1. Ferroxdure or BaM are the other names of M type barium hexaferrite [10]. BaM found its applications in magnetic recording media, permanent magnets and microwave devices [11].

1.4.1 Crystal Structure of M-type Barium Hexaferrite:

The composition of fundamental structural R and S blocks in BaM is $BaFe_6O_{11}$ and Fe_6O_8 respectively. R and S blocks are stacked in M type Barium hexaferrite to form a unit cell in sequence RSR*S* where the sign star denotes the 180^o rotation about the c-axis of the hexagonal lattice. Therefore, two $BaFe_6O_{11}$ molecules are present in the unit cell of BaM. Four oxygen ions are present in each of the two hexagonal layers in S Block while R block constitutes three hexagonal layers of oxygen. One oxygen ion in the middle hexagonal layer in R block is replaced by a barium ion. Five interstitial sites are occupied by the metal ions in the unit cell of BaM. The location of these sites, their sublattices, No. of ions and coordination's are mentioned in the table below [10]:

Table 1.5: Location, sublattices and Coordination of Interstitial sites in BaM

Block	**Sublattice**	**Coordination**	**Ions per unit cell**	**Spin direction**
S	$4f_1$	Tetrahedral	4	down
	2*a*	Octahedral	2	Up
R	$4f_2$	Octahedral	4	Down
	2*b*	Bi-pyramidal	2	Up
S-R	12*k*	Octahedral	12	Up

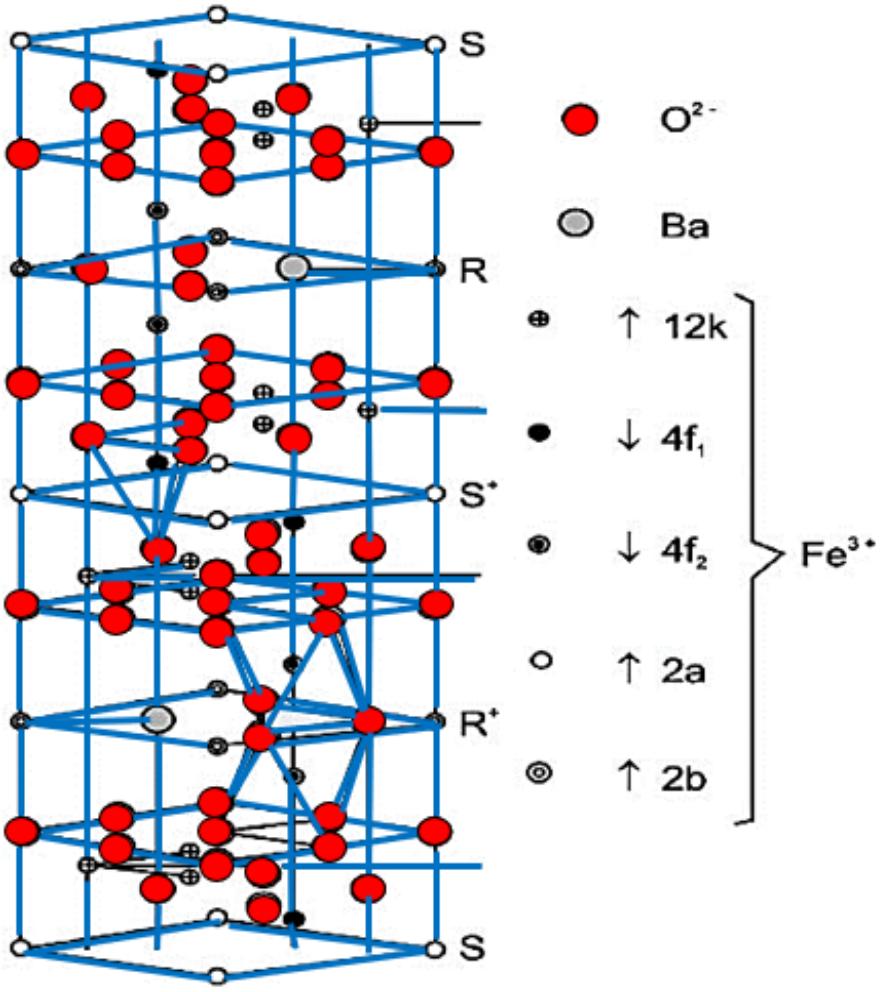

Figure 1.11: Unit cell of M type Barium Hexaferrite with the spin orientation of sublattices

1.5 Properties of Hexaferrites

Depending upon nature and composition, hexaferrites have various groups but they resemble each other because of some similarities in crystal structure. The main component in hexaferrite, which is responsible for the magnetic moment, is iron cations present at Tetra, Octa or Hexahedral sites. Few of physical, magnetic, dielectric and photocatalytic properties are discussed below:

1.5.1 Physical Properties:

Physical properties of hexaferrites vary greatly with composition. They have some excellent hard ferrite properties because of which they are often considered for making permanent magnetics. For the fabrication of microelectronics, ferrites are synthesized at higher temperature of around 900+^{o}C.

1.5.2 Dielectric Properties:

Dielectric properties mainly include dielectric constant, loss, tangent loss and ac conductivity, impedance and electric modulus. The information about the formulation of electric field in the material can be gained from these properties. In ferrites, electric hopping between Fe^{+2} and Fe^{+3} shows the prominent conduction mechanism.

1.5.3 Electrical Resistivity:

In hexaferrites, ferrous and ferric ions are present simultaneously on octahedral sites, causing the electrical resistivity. Depending upon the composition, electrical resistivity ranges from 10^{-2}-10^{11} Ohm-cm. Researchers have been working on improving the electrical resistivity of ferrites using various techniques. Doping is a well-tested technique for this purpose in which a very small amount of impurity or foreign ions are introduced in the oxides then these ions may force the already present ion into a different site owing to the difference in valences. Resistivity mainly depends on the number of ferrous ions: Lower the number of ferrous ions in stochiometric ferrites higher will be the resistivity. The general relation of resistivity with temperature for ferrites is given as

$$\rho = \rho_0 \, exp(E_a/kT)$$

Where ρ represents resistivity, T is temperature and Ea is the activation energy which is required for electron hopping between two ions and it usually lies between 0.1 to 0.5 eV. Higher the activation energy, higher will be the resistivity, as seen from the equation.

1.5.4 Conduction Mechanism

Owing to distinct electrical properties of ferrites, they are applicable for various electronic applications. The conduction mechanism in ferrites differ from

semiconductors as in ferrites the temperature affects the charge carrier mobility in turn effecting the conduction mechanism. Charge carriers in ferrites are localized at the magnetic atoms and carrier concentration in independent of temperature. Hopping of 3d electrons between Fe^{+2} and Fe^{+3} causes the conduction in ferrites. Closely packed oxygen anions surround the metal cations causing the isolation of electron to a particular ion and there is a small overlapping of anionic cloud or orbital. Due to isolation of each electron to a particular ion, localized electron model is more significant in ferrites as compared to band model.

1.5.5 Magnetic Properties

In large metal ions like barium and strontium, the size of crystal lattice is varied. This forms the basis of magneto-crystalline anisotropy which results in distinct magnetic properties in hexaferrites. The magnetization in most of the hexagonal ferrites is shown in the direction of c-axis because of which their XRD pattern differ from any other ferrites oriented in random order.

Magnetic properties of hexagonal ferrites can be altered by the addition of metal cations by doping. With the addition of metal cation like aluminum, gallium or chromium, the magnetic anisotropy and magnetization of barium hexaferrite can be enhances.

1.5.6 Photocatalytic Properties

Along with electronic and magnetic applications, ferrites can also be employed for photocatalytic applications. The narrow band gap of ferrites lies in the visible region hence they are suitable for visible light photocatalysis for the degradation of synthetic dyes like methylene blue and rhodamine B and can be separated using external magnet ensuring the reusability. Based on the high magnetic coercivity, saturation magnetization and thermal stability, hexaferrites lies in the class of hard ferrites. Using hexaferrite as catalyst with the addition of hydrogen peroxide H_2O_2, a Photo-Fenton type degradation system for dyes establishes [12].

1.6 Significance of ferrites

Because of the applications in electronics, ferrite materials are recognized as essential component for the development of electronic industry. After the thirty years of industrialization of iron-silicon alloy, commercialization of ferrites has started and gained attention in 1956's after the realization of expanding high frequency applications in television, microwave devices, radio and electronic circuitry [13]. Iron and its alloys possess low DC resistivity and thus can be used in various technologies but the applications like electronic circuitry and inductors cores, require high frequency limiting the use of iron alloys. However, ferrites, due to their high DC resistivity can be employed for such applications. Areas of applications including delay lines, electronic and filter circuit and adjustable inductors can also make use of ferrites because of their high permeability and temperature stability. Ferrites also offer mechanical stability, magnetic properties and cost effectivity, which none of other metallic materials can offer [1].

1.7 Applications of Ferrites

Ferrites have enormous number of applications ranging from millimeter wave integrated circuit to power handling, simple permanent magnets and magnetic recording media. Some of the applications of ferrites are listed below:

- Ferrites are an important component of engineering and technology because of their spontaneous magnetic moment below curie temperature.
- They can be employed in microwave devices as core of coils because of low eddy current losses.
- They found their use in computer memory core elements, data processing circuits and electrical circuits.
- They can be used in recording media as magnetic heat transducer.
- Ferrites can be employed in power limited and harmonic gyration devices.
- Hard ferrites can be used to make permanent magnets which can be employed in galvanometer, ammeter, voltmeter, flex meters, speedometers, wattmeter, compasses and recorders.

Other than the conventional applications, ferrites are also investigated for the novel applications in electronic industry and natural environment are:

- In electrically charged vehicles, ferrites can be used in magnetic parts of direct current driving motors.
- Washer disposal method for factory drains.
- Heat decomposition of CO2 using a mixture of carbon and ferrite powders heated at 300°–700°C
- Transformation of solar energy to hydrogen energy using ferrites as catalysts
- Heat decomposition of NOx gas using spinel ferrite [13].

1.8 Motivation of Work

This research work has following objectives:

- Synthesis of Barium Hexaferrite nanoparticles $BaFe_{12}O_{19}$ employing simple method of Sol-gel.
- Employing sol gel method for the Synthesis of Ni, Mn and Co substituted Barium Hexaferrite nanoparticles at various concentration.
- To investigate the effect of doping of Ni, Mn and Co on the electrical and magnetic properties of barium hexaferrite.
- Study of electrical and magnetic properties at different concentrations of dopant.

Chapter 2

Literature Review

K.S. Martirosyan et al. used carbon combustion method to synthesize crystalline barium hexaferrite nanoparticles with the average particle size of 50–100 nm. In this method, carbon has been oxidized in an exothermic reaction and the solid reactants are converted to barium hexa-ferrite as the thermal front propagates. When the carbon concentration reached 11wt%, a complete conversion of solid reactants to barium hexaferrite was observed. The magnetic coercivity and saturation magnetization value of the sintered sample came out to be Hc∼3000 Oe and Ms∼50.3 emu/g. [14]

Sunil Kumar et al. had synthesized chromium doped barium Hexa-ferrite using modified sol-gel method. Various concentrations of chromium were used to evaluate the effect of doping on various properties. XRD results confirmed single phase nanocrystalline structure with no impurity phase. Magnetic hysteresis loop was obtained using Law approach to saturation method, revealing the ferromagnetic nature. Magnetic coercivity and anisotropy seemed to increase as the chromium concentration increases. [15]

M. Radwan et al. utilized the co-precipitation method to synthesize nanocrystalline barium hexa-ferrite followed by high temperature calcination. Barium and iron chloride precursors were used along with sodium hydroxide as precipitating agent. The precursors were calcined at high temperature and structural and magnetic properties were studied. It was found that by decreasing the molar ratio of Ba^{+2}/Fe^{+3}, single phase barium hexaferrite can be achieved. Magnetic coercivity and saturated magnetization values were (642.4–4580 Oe) and (50.02) emu/g respectively. [16]

Daming Chen et al. Investigated the sol gel method for the synthesis of aluminum doped barium hexaferrite and its effects on magnetic coercivity, anisotropy and saturation magnetization. Sodium citrate was used as chelating agent and calcination was performed at higher temperature. XRD analysis confirmed the presence of aluminum in Fe sites as a result of substitution. SEM analysis showed that the morphology of barium hexaferrite s the effected by doping of aluminum. However, a decrease in saturation magnetization was observed with increase in concentration of

dopant. In addition, magnetic coercivity and anisotropy seemed to be increased by increasing the molar ratio of sodium citrate and barium ions. [17]

H. Sözeri et al. investigated the substitution of divalent and trivalent metallic cations in barium hexaferrite to form a complex compound $BaFe_{10}M^{+2}Ti^{+4}O$. Solid state reaction method was used for synthesis along with a growth inhibiting compound at lower temperature and XRD, SEM, magnetization and near field microwave measurements were performed. Saturation magnetization seemed to be decreased with the substitution of cation. Dielectric constant was increased after the substitution of $Zn^{2+,}$ $Mn^{2+,}$ Co^{2+} and Cu^{2+}. Minimum reflection loss for microwave absorption came out same for all the samples. [18]

Pratap Behera et al. carried out a study in which nickel doped barium hexaferrite was synthesized by sol-gel method to form a single-phase polycrystalline sample. Dielectric properties were investigated using impedance spectroscopy at various frequencies to understand the relaxation mechanism of charge carriers. With increasing nickel concentration, dielectric constant seemed to increase while the tangent loss decreased. However, saturation magnetization decreased, and the transition temperature increased with increasing nickel concentration. [19]

Hossein Nikmanesh et al. carried out a study in which a nanocomposite of carbon nanotubes with barium hexaferrites doped with copper, magnesium and zirconium was synthesized using chemical route based on two stages. XRD analysis was performed the confirm the successful synthesis of nanocomposite. The structure of carbon nanotubes was not destroyed after acid treatment and nanoparticles are absorbed on the surface of CNT's as confirmed by SEM and TEM analysis. Saturation magnetization obtained from VSM analysis showed an increase in value first and then decreased with increase of dopant concentration. Dielectric constant has the highest value for the samples with MWCNT's and reflection loss is minimum for the sample with high dopant concentration. [20]

S.H. Mahmood et al. investigated the synthesis of Barium hexaferrite doped with molybdenum and zinc using high energy ball milling method. Calcination was performed at different temperatures. For the sample sintered at $1100^{o}C$, the saturation magnetization decreased mainly due to the presence of nonmagnetic oxides. A

decrease in magnetic coercivity and increase in saturation magnetization was observed as the sintering temperature was increased. [10]

Sahel Mesdaghi et al. investigated the sol-gel auto-combustion method for the synthesis of M-type Barium hexaferrite nanoparticles doped with zinc, cobalt and tin and these nanoparticles were than decorated on multiwalled carbon nanotubes. Another composite was synthesized with polyaniline through in-situ polymerization. X-ray diffraction analysis was performed for phase analysis, morphology was studied from scanning electron microscopy images, magnetic properties were studies using VSM and catalytic activities of the prepared sample were evaluated by UV irradiation. Results revealed that $BaZn_{0.2}Co_{0.2}Sn_{0.4}Fe_{11.2}O_{19}$ was a potential candidate for magnetic separation as it possessed considerably high saturation magnetization. The composite of MWCNT's with $BaZn_{0.2}Co_{0.2}Sn_{0.4}Fe_{11.2}O_{19}$ showed maximum degradation of methylene blue. [21]

Reza Shams Alam et al. investigated co-precipitation method for the synthesis of barium hexaferrite doped with magnesium, cobalt and titanium. A composite of acid treated MWCNT's with BaM was prepared through sonication. Vibrating sample magnetometer analysis was performed to study saturation magnetization and coercivity which were seemed to be strongly related to concentration of MWCNT's. [22]

Varsha C. Chavan et al. sol gel was used for synthesis of M-type barium hexaferrite Ba1-xCoxFe12O19 where x changes from 0.0-1.00 having steps of 0.25 post annealing was done at 600°C. FTIR, XRD, SEM and vibrating sample magnetometry were used for characterization. Transformation of crystal to spinel from pure barium hexaferrite with substitution of Co2+ was observed. SEM analysis show regular grains and well define structure. Crystal symmetry obtained through XRD is supported by FTIR spectra. Decrease in saturation magnetization and magneton number while increased coercivity by doping of Co2+ showed through magnetization results. [23]

Kajal K. Mallick et al. synthesized M-type barium hexaferrite doped wit cobalt with various concentrations using co-precipitation and solid-state reaction methods. The purpose behind this synthesis was to improve the magnetic properties and permeability values. XRD analysis was performed to confirm the doping of cobalt in Fe sites while the density of the obtained samples varied with concentration with maximum density

of 4.45g/cm^3. Saturation magnetization value reduced from 87-58emu/g while the coercivity value largely increased from 540-2200Oe. [24]

Shalini et al. studied the magnetic properties of pure and cobalt doped barium hexaferrite nano powders synthesized through modified sol-gel auto-combustion method. Saturation magnetization value seemed to decrease from 60emu/gm to 54emu/gm at the temperature of 300K. Similarly, the coercivity value was also decreased with doping. Whereas, when the temperature was decrease from 300K-60K, saturation magnetization value started to increase. Coercivity of undoped and doped sample was found to decrease and increase at 60K, respectively. [25]

Moaz Waqar et al. investigated the effect of doping of Nickel in barium hexaferrite on magnetic properties. Sol-gel method was utilized for the synthesis and XRD-analysis was performed to confirm single phase impurity free sample. Magnetic properties were studied using vibrating sample magnetometer and results showed an increase in saturation magnetization with the doping of nickel. Magnetic coercivity was decreased with doping of nickel with various concentrations ranging from $x = 0$ to $x = 0.5$. Permittivity, dielectric loss and conductivity of the sample was also studied and reported. [26]

Chapter 3

Materials and Methods

3.1 Synthesis Routes for Ferrites

The two basic approaches used for the synthesis of nanoparticles include:

- Top down approach
- Bottom up approach

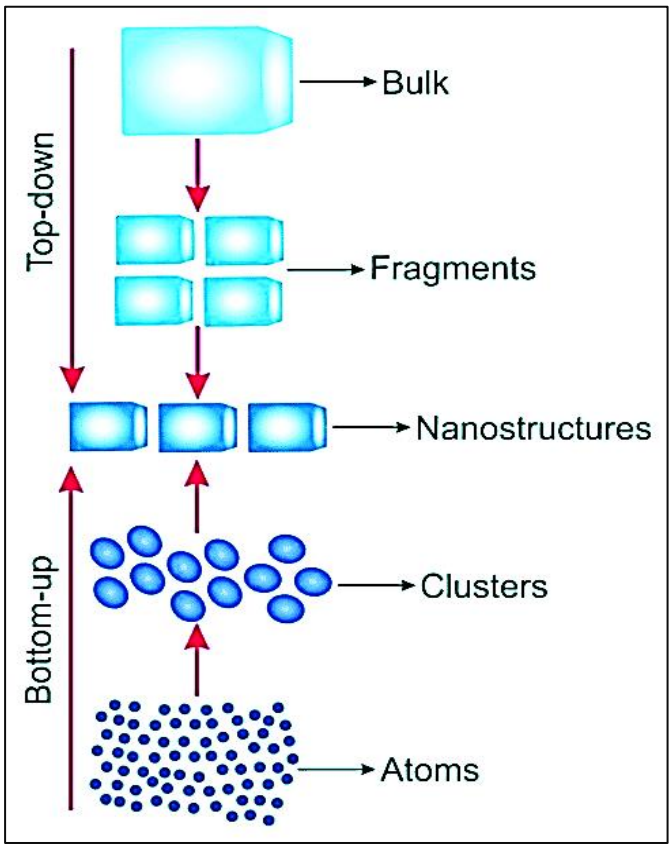

Figure 3.1: Schematic representation of fabrication of nano-structures using Top down and Bottom Up approach [27]

3.1.1 Top Down Approach

In this approach, Macroscopic initial structures are utilized and scaled down to fabricate many man-made materials including the semiconductor industry. The typical example of this technique is lithography which is employed to print metal oxide field effect transistor onto silica wafer. Apart from advantages, the product obtain from top down approach might contain significant amount of impurity.

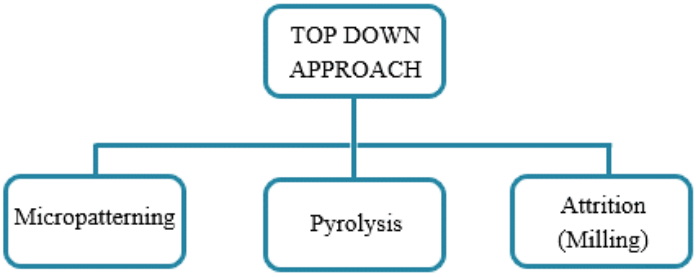

Figure 3.2: Example of top down approach

3.1.2 Bottom-Up Approach

In contrast to top down, atoms and molecular are gathered to form nanoparticles which can be used to fabricate various intelligent nanodevices. The drive behind the development of bottom-up approach is to mimic the self-assembled and self-organized preprogrammed biological structures and the supramolecular chemistry involved to combine those structures.

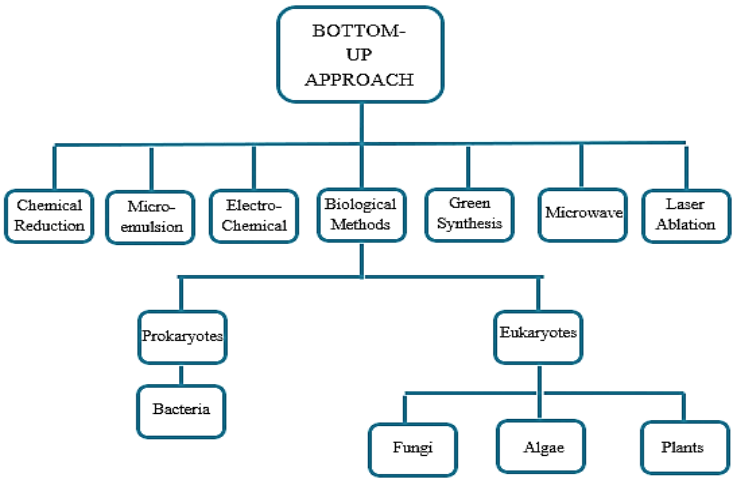

Figure 3.3: The examples of bottom up approach

Synthesis of nanoparticles with nano dimensions have become very difficult task for many researchers. To obtain monodispersed nanoparticles, various methods have been adopted. These are listed as below.

3.1.2.1 Solid State Method

In this method the constituent products are mixed collectively under elevated temperature. These methods are specifically employed for obtaining bulk material. Solid state reactions are often very slow, and their completion occurs at very elevated temperature. The ferrites in bulk form are prepared through this method with size ranging in microns. Solid state approach also has some short comes such as chemical in-homogeneity, compositional control is poor, particle size is not fine and risk of impurities during grinding. To overcome these shortcomings chemical methods are implemented.

3.1.2.2 Chemical Method

In this method the aqueous solution of the constituent's salt is used. The obtain solutions of these materials are then dried and fine powder is achieved. This method is also termed as wet method. The wet method or chemical methods have their advantages to design and manufacture new materials for refinement into final products. The main advantage of chemical method is its chemical homogeneity. This method is based upon mixing of constituent at molecular level. Besides these advantages some hurdles also arise in chemical processing due to complex chemistry and hazardous nature. In some cases, contamination may result from by product being produced or some side reactions may take place. Agglomeration can cause severe problems in any step of synthesis & development and significantly changes properties of material. Fine nanoparticles can be synthesized by precipitation from precursor solutions which is common technique for the synthesis. When the supersaturated solution is formed, precipitates are formed either by homogenous or heterogeneous nucleation. By the process of diffusion, nucleation takes place. The concentration slope and the temperature of reaction are key factor to determine the growth rate of mono dispersed nanoparticles. Narrow size distribution is needed for un-agglomerated preparation of particles such that all the simultaneous formation of nuclei and their

growth must occur subsequently. Kinetics of reaction is influenced by preventing nucleation or agglomeration of the particle, distribution of the particle size, crystallinity, crystal structure and degree of dispersion. Also, the concentration of constituents, temperature of reaction, sequence of mixing of the reactant and the pH are also essentials. To obtain chemical homogeneity and stoichiometry it is required to have careful controls on reaction conditions. In recent years the non-convention methods are widely used for obtaining ferrite nanoparticles due to the net advantages such as homogeneous distribution of ions at molecular level, high purity of resulting products and 100% efficiency, compare to usual solid-state reaction process. Particle size of the ferrite nanoparticles is key parameter, playing key role to determine the magnetic and electrical properties.

Different methods in preparing ferrite nano particle are listed below.

- Sol-Gel Method
- Combustion Flame Synthesis
- Co-Precipitation
- Mechanical Alloying Technique
- Micro Emulsion Method
- Sono-Chemical Method
- Hydrothermal Method

In our research work Sol-gel method was employed successfully for preparation of $BaFe_{12-3x}(Mn, Ni, Co)_x O_{19}$ ferrite nano particles.

3.2 Sol-Gel Method

Sol-gel method is utilized in this study to synthesize M-type Barium Hexaferrite doped with manganese, cobalt and nickel at x = 0, 0.2, 0.35, 0.5. During the process, a gel is formed which provided high degree of homogeneity and the diffusion of atom is reduced in the solid-state calcination. This technique provided better control on products and cost effective. The materials which are made through this technique have wide applications in optics, electronics and energy etc.

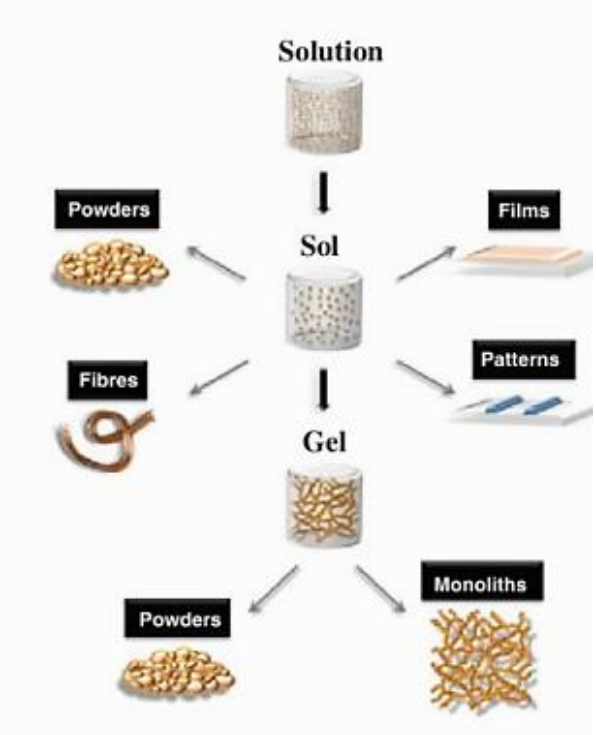

Figure 3.4: Sol-gel method to synthesize various forms of materials [28]

3.3 Experimental Details

Below are the details of the experiment carried out to prepare the desired sample.

3.3.1Materials:

Table 3.1: Chemicals

Serial. No.	**Name of Chemical**	**Formula**
1	Barium Nitrate	$Ba\ (NO_3)_2$
2	Iron Nitrate Nonahydrate	$Fe\ (NO_3)_3.9H_2O.$
3	Cobalt Nitrate Hexahydrate	$Co\ (NO_3)_2.6H_2O.$
4	Manganese Nitrate Hexahydrate	$Mn\ (NO_3)_2.6H_2O.$
5	Nickel Nitrate Hexahydrate	$Ni\ (NO_3)_2.6H_2O$
6	Citric Acid	$C_6H_8O_7$
7	Ammonia Solution	NH_4OH

Initial reagent to synthesize all the salts is deionized water. All the chemicals used for samples preparations in this study were of purity ≥ 99% and were used without any further purification.

3.3.2 Synthesis of Barium Hexaferrite ($BaFe_{12}O_{19}$)

Sol-gel method was used to synthesize $BaFe_{12}O_{19}$ and the stoichiometric formula that was used to calculate mass for three different compositions of different chemicals utilized in the process is as follows:

$$\frac{Molarity \text{ x } Molecular\ mass \text{ x } 100}{1000} \quad \ldots\ldots\ldots\ldots\ldots\ldots\ldots\ldots \quad (3.1)$$

Solution of Barium nitrates Ba $(NO_3)_2$ and iron nitrate (III) nonahydrate Fe $(NO_3)_3.9H_2O$ were prepared according to their stoichiometric ratios. Ba $(NO_3)_2$, Fe $(NO_3)_3.9H_2O$ were dissolved in 100ml of deionized water by constantly stirring using a magnetic stirrer for 15 minutes for their complete dissolution and to get clear solution in water. 100ml of deionized water was taken to dissolve citric acid and was stirred until solution get clear and complete dissolution took place. In a large beaker both solutions were added with continuous stirring using magnetic stirrer and after 15 minutes of stirring pH was neutralize by adding ammonia solution.

Continuous stirring of solution was done and then the solution was heated at 90°C is powered ON, with the same condition of stirring. After some time, the solution started to change in to gel form. Finally, the thickened gel catches fire in beaker and once the combustion was completed, heating and stirring was turned off.

Dark brown colored powder was obtained after combustion. The powder was grinded in mortar and pestle and then calcination of the collected powder was done at 950^{o}C for 5 hours.

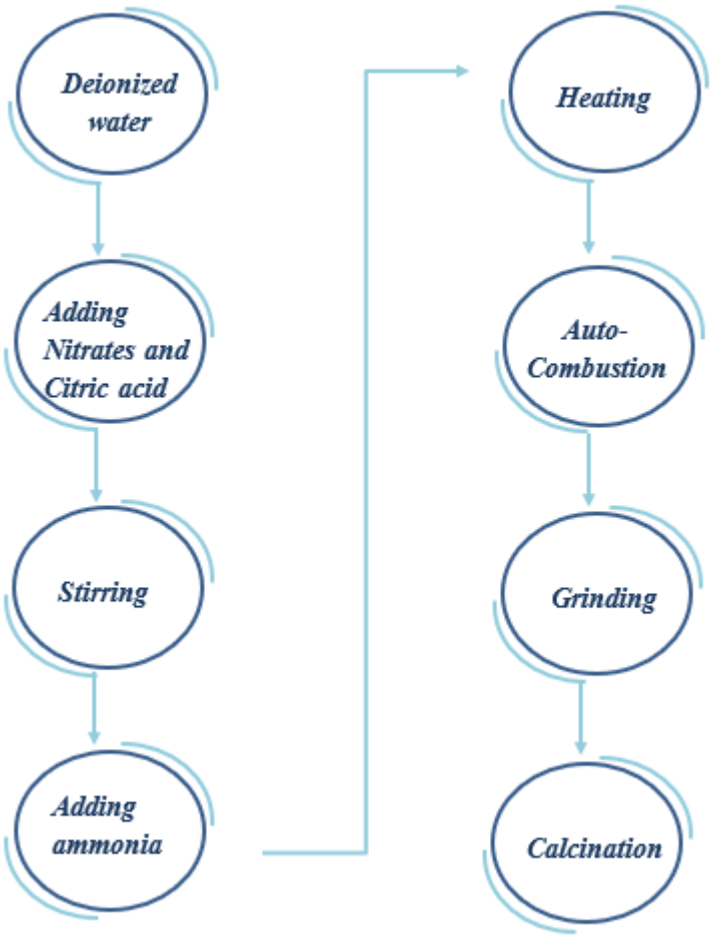

Figure 3.5: Flow chart of the Synthesis of Pure Barium Hexaferrite

3.3.3 Synthesis of $BaFe_{12}O_{19}$ Doped with Manganese, Nickel and Cobalt Dopant

Series of sample preparation with cobalt, nickel and manganese as a dopant was prepared. The sample series [$BaFe_{12-3x}$ (Mn, Co, Ni) $_x$ O_{19}] for x=0, 0.2, 0.35, 0.5, were prepared. Samples were prepared in 600 ml of deionized water by adding Ba $(NO_3)_2$, Fe $(NO_3)_3.9H_2O$, Co $(NO_3)_2.6H_2O$, Mn $(NO_3)_2.6H_2O$, Ni $(NO_3)_2.6H_2O$ and citric acid according to their stochiometric ratios by sol-gel technique. The solution was continuously stirred for 15 minutes with magnetic stirrer until the complete dissolution took place solution became clear. Dropwise solution of ammonia was added until the pH reaches 7 with continuous stirring.

Solution was stirred continuously with magnetic stirrer and then heating at 90 °C temperature is powered ON, with the same condition of stirring. After some time, the

solution started to change in gel form and after thickened gel catches fire in beaker and after complete combustion the heating and stirring is stopped.

After combustion, dark brows colored powder was obtained. Grinding was done in mortar and pestle and then placed in muffle furnace at 950 °C for 5 hours for calcinations purpose.

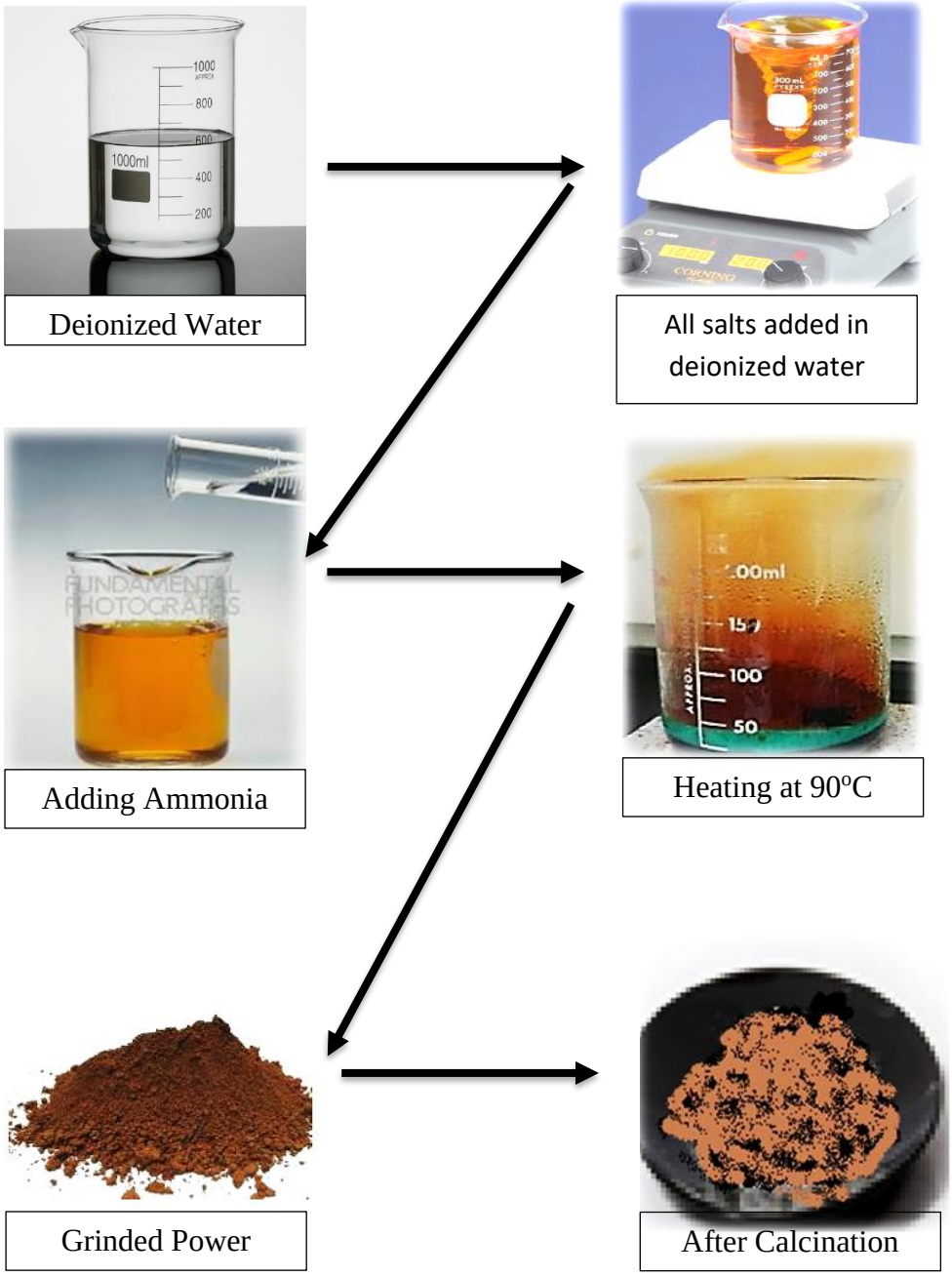

Figure 3.6: Flowchart of Synthesis of BaM doped with Mn, Ni, Co

Chapter 4

Characterization Techniques

The properties of synthesized nickel ferrite nanoparticles with graphene loadings are analyzed by performing some specific analysis techniques. Properties like physical and chemical properties and other information about material such as morphology, lattice parameter, structure etc. can be obtained using one of the analysis techniques. This chapter will cover a short introduction of the characterization techniques. Following characterization techniques can be used for the analysis of synthesized composite.

4.1 X-Ray Diffraction Technique

It is a useful tool for the identification of degree of crystallinity and structure of a material. Clear information about structural strain, crystal defects, average crystallite size, crystallographic orientation and degree of crystallinity can be obtained using XRD [29]. Three different methods can be used for finding out crystal structure i.e. Powder diffraction method, Laue method and Rotating crystal method.

Two techniques can be used to determine crystal size if powder diffraction method is used. Those techniques are as follows.

- Debye Scherrer Method
- Diffractometer method

The sample was in the form of fine grinded powder. Copper, Molybdenum etc. can be used as a target material. Cu k-alpha=1.54 Å source was the XRD source used for analysis in this case.

4.1.1 Basic Principle of XRD

The powdered sample is placed for analysis. X-ray beam is made to fall on the sample and reflected from plane of crystal. The crystal plane reflects the X-rays that are incident on material. The interference only takes place when incidence angle is exactly same as reflection angle. The Bragg's Law is given by

$$n\lambda = 2d\sin\theta \quad \text{.....(4.1)}$$

n is order of interference, θ is incidence angle, d is Interlayer distance and λ is incident X-ray wavelength. The Bragg's law states that the incident ray is reflected only when the path difference between set of planes is 2dsinθ [30]. The set of planes are at an equal distance of d. Following is the condition required for constructive interference:

$$2d\sin\theta = n\lambda, \text{ where } n=1,2,3\ldots..$$

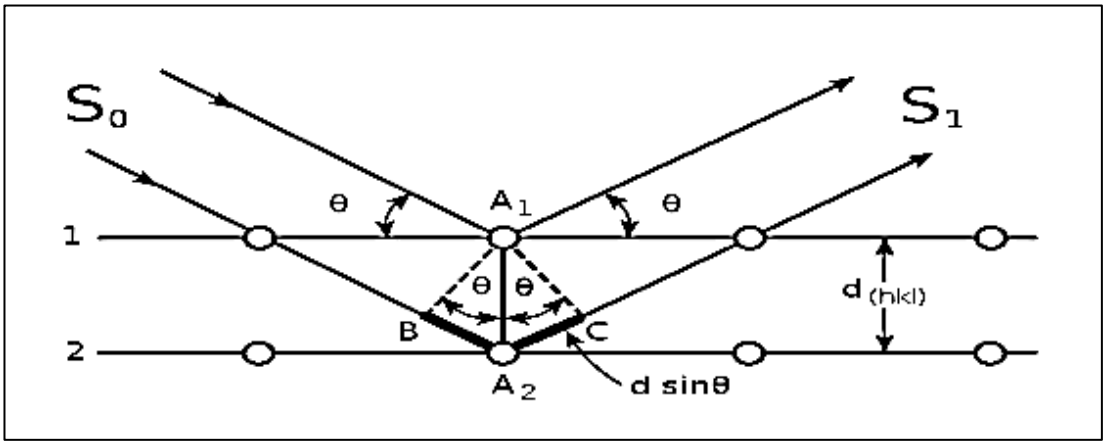

Figure 4.1 Incident x-ray beam scattered by atomic plane in a crystal [1]

The equation is known as Bragg's equation. The condition for reflection in above mentioned equation is that it only occur when θ<2d. For this reason, visible light cannot be used. For the characterization of a three-dimensional structure three techniques are usually used which are as follows:

- Laue Method
- Powder method
- Rotating Crystal Method

The sample which is to be characterized using XRD is in the form of Nano powder. So, the powder method will be the one useful for the desired sample. For the evaluation of powdered sample and in the case of in availability of single crystal of acceptable size, powder diffraction is the best method to be employed. The procedure of this experiment includes the crushing of sample into fine powder. Afterwards the sample will be placed in aluminum or glass rectangular shaped plate. A monochromatic X-ray beam is then directed towards the powdered sample.

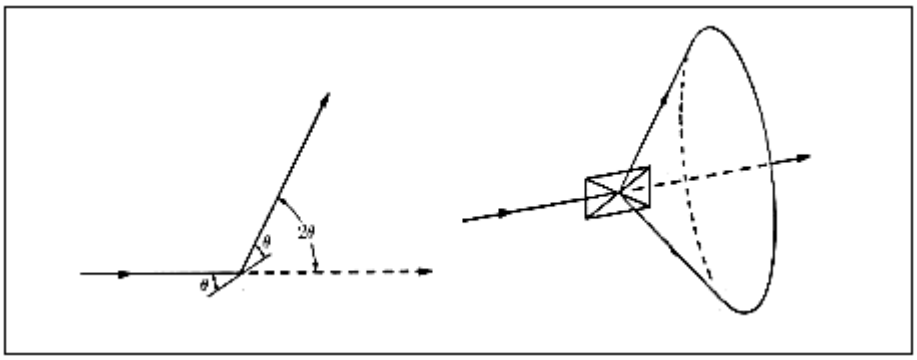

Figure 4.2: X-ray Diffraction [1]

Consider the reflection as shown in figure. The fraction of sample, which is in powder form, is at such an orientation which will enable reflection by being present at correct Bragg angles. When the plane is rotated about the beam which is made incident, the path of motion of reflected beam will be across the surface of cone. In the case of our particles the reflection does not occur across the surface, a large number of crystal particles will have same reflections and some of those reflections will be able to satisfy brags law. The inter planner spacing, d, can be calculated by knowing values of λ and θ.

4.1.2 Lattice constant

Lattice constant defines the unit cell of a crystal. It is the length of one edge of the cell or an angle forming between edges. It can also be termed as lattice constant or lattice parameter. The distance, which is constant, between the lattice points is known as lattice constant. Following equation is used to calculate lattice constant.

$$\frac{1}{d^2} = \frac{4}{3}\left(\frac{h^2+hk+k^2}{a^2}\right) + \frac{l^2}{c^2} \quad \text{..... (4.2)}$$

In the above equation, lattice constant is “a”, the wavelength of X-ray radiation is 1.54 for Cu-kα, miller indices are “h, k, l” and diffraction angle is θ.

4.1.3 Crystallite size

For the identification and confirmation of the experimentally obtained diffraction pattern it is compared to JCPDS cards. The structural properties are greatly influenced by particle size. According to Debye Scherrer equation, which is used to calculate particle size, crystal size is inversely proportional to peak width. So, the small crystallite size is related to peak broadening in XRD analysis. The Debye Scherrer equation is used to calculate particle size.

$$t = 0.9\,\lambda/\beta\,cos\theta \qquad (4.3)$$

λ represents the incident X-ray wavelength and θ and β represent diffraction angle and full width half maximum respectively.

4.1.4 X-Ray Density

The X-ray diffraction data can be used for the calculation of sample material's density [31].

If the lattice constant is known for each sample following formula will be used.

$$\rho x = 8M/Na^3 \qquad (4.4)$$

Where ε represents molecular weight of sample, N is the Avogadro's number ($6.03x10^{23}$) and "a" is the lattice constant. Eight formula units are possessed by each cell.

4.1.5 Measured Density

The intrinsic properties of materials define the bulk density or measured density. The density formula is generally used for the density calculation.

$$\rho_m = m/\pi r^2 h \qquad (4.5)$$

Where m represents the mass, r represents the radius; h is the thickness of the pressed pellet sample. For the calculation of measured density, a circular pallet is made using hydraulic press which compact the powdered sample. Vernier caliper is used for measuring thickness and radius of pallet and analytical balance is used for measuring

mass of the pallet. The measured parameters are substituted in equation for the resultant density calculation.

4.1.6 Porosity Fraction

Along with the alternation in compositions, the increase in the porosity fraction is observed. Following formula is used for calculation of porosity fraction.

Porosity Fraction = I – $\rho m/\rho x$ ………………………….... (4.6)

4.2 Fourier Transform Infrared Spectroscopy

The absorption, emission spectra's, Raman scattering, and photoconductivity of the material can be obtained by using this analytical technique. The stretching modes of the elements present in composite and chemical purity of the sample can be determined using FTIR. It is known as FTIR because it involves the Fourier, a mathematical term. It collects the data from spectrum of matter. FTIR is used to determine the amount of light that a sample absorbs at a specific wavelength.

4.2.1 Working of FTIR

In Fourier transform infrared spectroscopy, a source of infrared light which is polychromatic is made to fall on splitters. Half portion of the incident light is refracted towards fixed mirror and other half of the incident light is transmitted through a moving mirror. Transmitted light passes through the sample. The information about molecular component and structure of the sample can be obtained by interaction of light with sample.

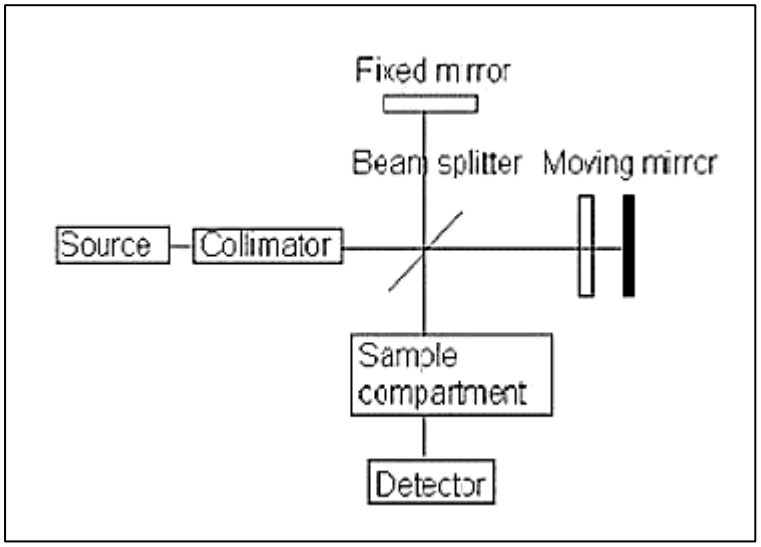

Figure 4.3: Schematic Figure of Fourier Transform Infrared Spectroscopy

It is a sensitive technique and can also be used for identification of many organic compounds for example, paints, polymers, resins, coatings and drugs etc. it is the only analytical technique which provides ambient temperature operation and capability of monitoring the vibrations of functional groups directly, which are used for characterizing molecular structure and governing the course of chemical reactions. [32]

IR radiation lies between the microwave and visible portions of electromagnetic spectrum and have wavelength longer than that of visible and shorter than microwaves. The frequencies of IR radiations are lower than visible and higher than microwaves. The IR region can be divided into; near, mid and far IR regions. Near-IR refers to the part of IR spectrum closest to visible light and far-IR refers to the part closer to the microwave region. While the mid-IR is the region lying between these two. The primary source of IR radiation is thermal radiation and it is produced as the result if motion of atoms and molecules in the sample. The higher the temperature, more the atoms move producing more IR radiations.

According to the principle of FTIR, molecular vibrations are produced because of absorption of IR radiation when the applied IR frequency is equal to the natural frequency of vibration. Different frequencies are required by every different bond or functional groups for absorption. Therefore, the characteristics peak is observed for every functional group or part of the molecule. [33]

4.2.3 Applications of FTIR

A gas chromatograph is used to separate the components of a mixture

- The analysis of liquid chromatography fraction can be done using FTIR.
- Tiny samples can be checked with the help of infrared microscope in sample chamber.
- The sample acquiring emitted spectrum of light is obtained FTIR instead of light spectrum through the sample [34]

4.3 Electrical Properties

Dielectric properties are measured using impedance analyzer pellet is placed in pellet holder and connected to device.

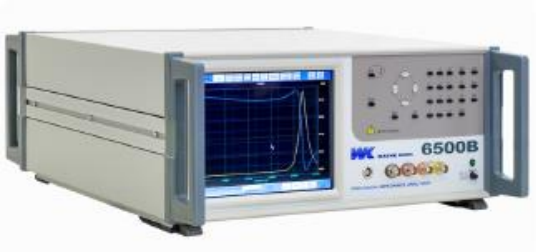

Figure 4.4: Impedance analyzer

4.3.1 Dielectric Properties

The LCR meter bridge is used for determination of dielectric properties such as dielectric loss, dielectric constant etc. Firstly, the capacitance of pallets was found out using LCR meter then following formula is used for the calculations of dielectric constant.

$$z = Cd\ A\epsilon o \quad \text{……..……(4.7)}$$

Where ϵ' is permittivity of material which represents its ability to store charge, C represents the capacitance of the pellet (farad), t represents the thickness of the pellet (Meters), A represents the cross-sectional area of the flat surface of the pellet and ϵo is the constant of permittivity for free space and its value is equal to 8.85x10-12 F/m. The imaginary part that corresponds to the energy dissipation losses is calculated by using the following equation:

$$\epsilon'' = \acute{\varepsilon} \times D \ldots\ldots\ldots\ldots\ldots\ldots\ldots\ldots\ldots\ldots\ldots\ldots\ldots\ldots (4.8)$$

Where $\epsilon''$is dielectric loss of material and D represents the dissipation factor. There are different types of polarization which take place in dielectric materials when the Interact with the applied field.

4.3.2 Electronic and Atomic polarization

When the dielectric material is placed within the electric field the electron cloud of atoms is displaced relative to nuclei in atom, which produce an induced dipole moment in the molecule.

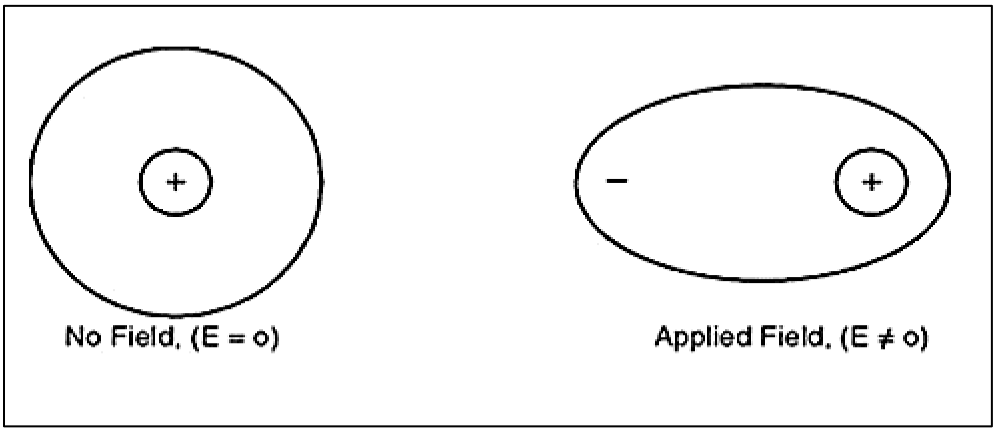

Figure 4.5: Electronic polarization [31]

4.3.3 Ionic Polarization

Ionic polarization take place in solids with ionic bonding having dipoles, but these dipoles get cancel due to the symmetry of the crystals structure. In the presence of applied electric field positive and negative ions are displaced from their equilibrium positions hence inducing dipole moment.

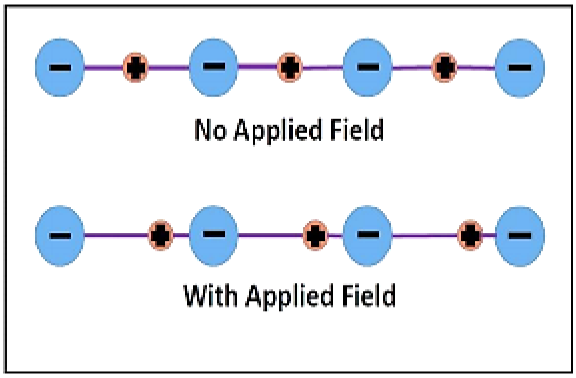

Figure 4.6: Electronic polarization [31]

4.3.4 Dipolar and Orientation Polarization

It is only applicable to the polar dielectric materials. In the absence of electric field dipoles are randomly oriented so the sum of their dipole moment is zero. When these polar dielectric materials are placed within the electric field these dipoles rotate and align themselves in the direction of electric field.

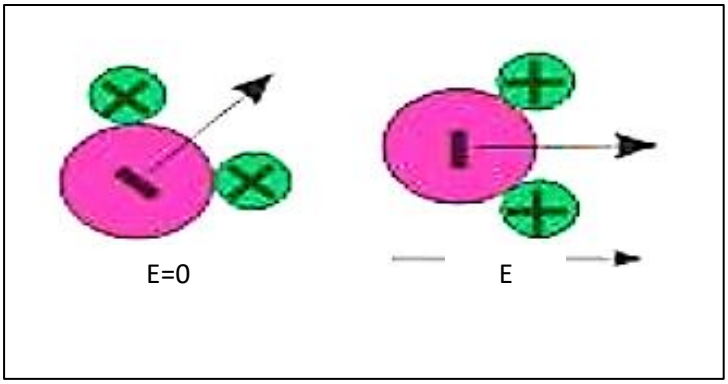

Figure 4.7: Dipolar Polarization [31]

4.3.5 Interface and Space Charge Polarization

Space charge polarization take place due to the diffusion of ions along with applied electric filed. It usually occurs due to the accumulation of charges in the interface or at the grain boundaries of the material.

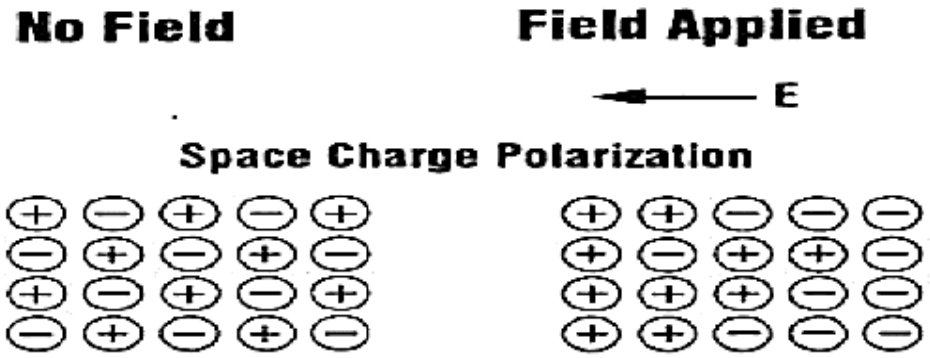

Figure 4.8 Space Charge Polarization [31]

4.4 Vibrating Sample Magnetometer (VSM)

Simon Foner, in 1959 designed the first Vibrating sample Magnetometer at Lincoln Laboratories. Its main purpose is to measure the routine magnetic properties at varying temperatures for all type of magnetic materials like Ferrimagnetic, Ferromagnetic, anti-ferromagnetic, diamagnetic and paramagnetic.

4.4.1 Principle

Vibrating sample magnetometer work on the principle of Faraday's law of Induction according to which a homogeneous magnetic field is applied on the sample and is vibrated at a small fixed amplitude. The pick-up coils are stationary with respect to vibrating sample. The change in applied magnetic field generates voltage in stationary pick-up coils.

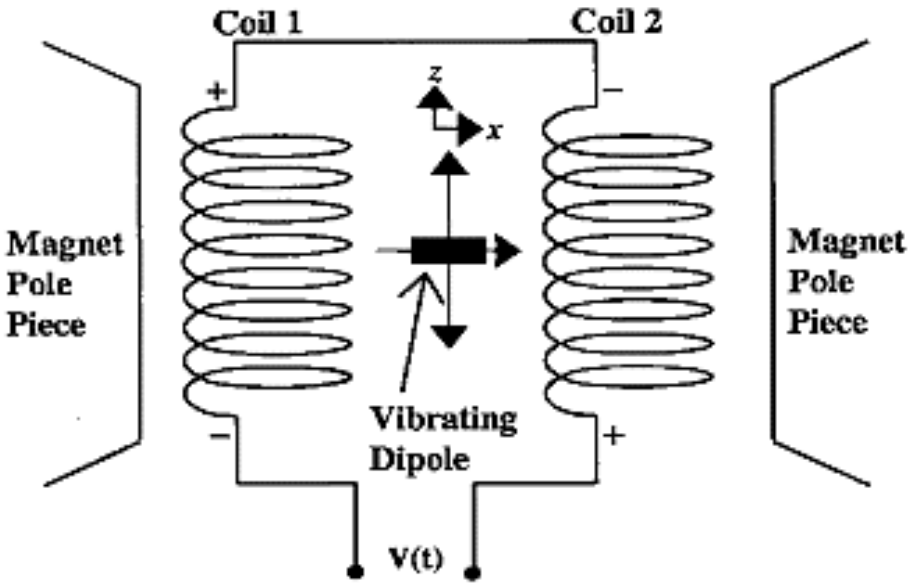

Figure 4.9: Principle of Vibrating Sample Magnetometer [35]

4.4.2Parts of VSM

4.4.2.1 Water Cooled Electromagnet

The constant magnetic field used to magnetize a sample is provided by water cooled electromagnet along with power supply.

4.4.2.2 Sample Holder and Vibration Exciter

A sample rod is used to hold the sample between pick-up coil pole pieces. Sample rod is attached to a vibration exciter which vibrate the sample with a fixed frequency. Different orientation of the sample can be exposed to constant magnetic field by rotating the sample rod. Oscillation of the vibration exciter is controlled by a chassis.

4.4.2.3 Sensor coils and Amplifier

As the sample is vibrated at a fixed frequency, alternating current is generated in these sensor coils. Signals generated through sensory coils are amplified by the attached amplifier to confirm the magnetization of the sample.

4.4.2.4 Lock-in Amplifier

This amplifies the signals by removing the noise coming from environment and only catches the signals only vibrating sample.

4.4.2.5 Computer interface

Data collection is made easier by the use of the software as it controls various components during the process. [36]

Chapter 5

Results and Discussion

5.1 XRD Analysis

XRD analysis was performed for phase testing and structural information. The sample was finely grounded and annealed at 950^{o} C before subjecting to XRD analysis.

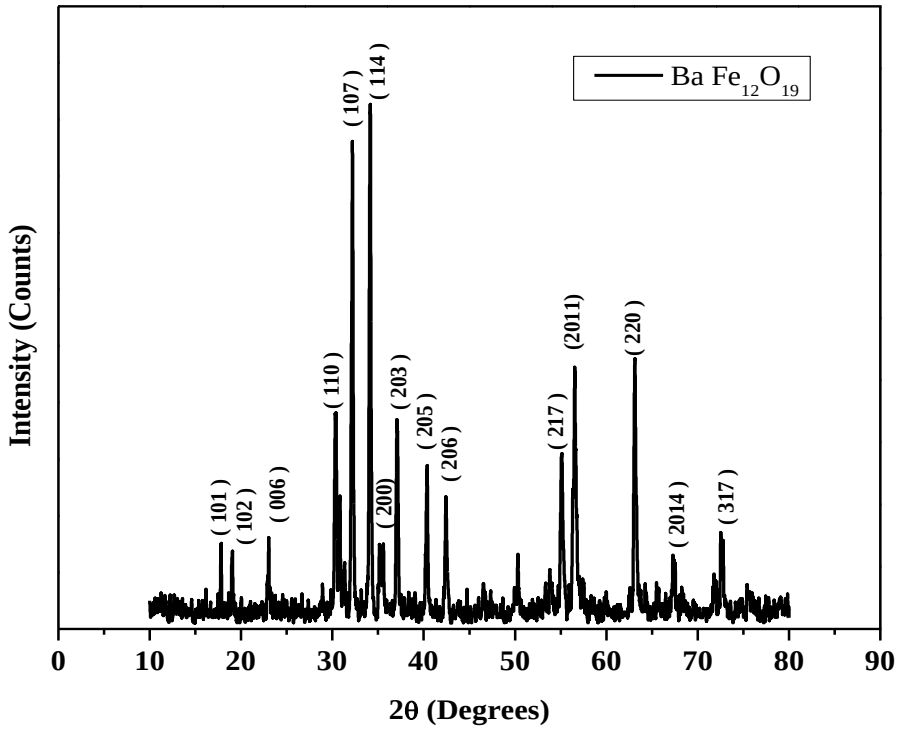

Figure 5.1: XRD Pattern of Pure Barium Hexaferrite

Fig 5.1 represents the XRD peaks of pure barium hexaferrite. The well-separated diffraction peaks for all the samples appear at planes (101), (102), (110), (008), (107), (114), (200), (203), (205), (206), (209), (217), (303), (304), (20 11), (220), (20 14), and (317) present at angles of 2θ = 17.784, 18.988, 30.315, 30.831, 32.196, 34.113, 35.146, 37.078,40.316, 42.422, 50.295, 55.057, 55.256, 56.326, 56.598, 63.06, 67.362 and 72.585 respectively. The pattern of peaks at specific angle matches with JCPDS data card No. 84-0757. The absence of any secondary peak confirms that there is no

extra hematite phase. Hence shows the completion of the reaction. XRD analysis shows the barium hexaferrite nanoparticles exhibit a single-phase hexagonal structure.

5.1.1 Barium Hexaferrite Doped with Mn, Co, Ni [$BaFe_{12-3x}O_{19}$]:

The Barium hexaferrite was doped with Manganese, Cobalt, and nickel with various concentrations where x = 0, 0.2 0.35, 0.5 using the sol-gel method for synthesis. XRD analysis was performed for the prepared doped samples after annealing at 950° C. The miller indices h, k, and l of the XRD peaks for the synthesized compound matches with the barium hexaferrite JCPDS data card No. 84-0757.

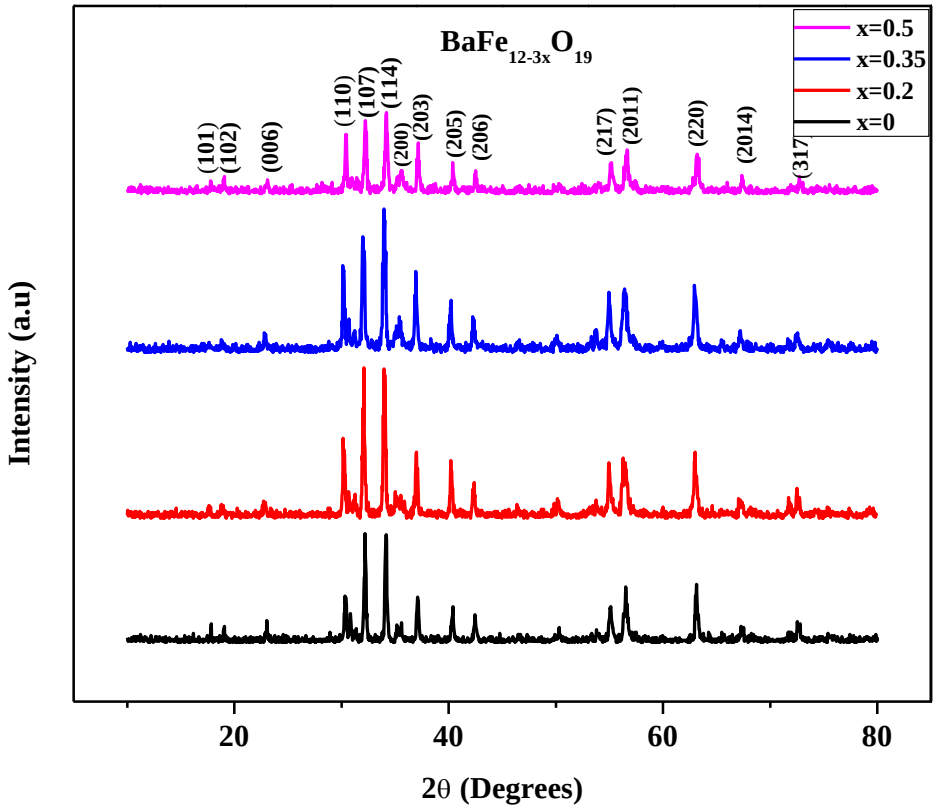

Figure 5.2: XRD Pattern of MNC Doped Barium Hexaferrite $BaFe_{12-3x}O_{19}$

There is no separate peak found after the doping of metallic cations Mn, Ni, and Co because of minimalistic difference in ionic radii of Fe^{+3} and Mn^{+2}, $Ni^{+2,}$ and Co^{+2}. The ionic radii of Fe^{+3} is 0.60A° while the ionic radii of Mn^{+2}, Ni^{+2} and Co^{+2} is 0.70

A^o,0.69A^o, 0.70 A^o respectively. so, as the ionic radii of three metallic cations and iron were comparable suggesting that the cations replaced iron-on tetrahedral sites.

The following relation was used to calculate the lattice parameters of pure and doped samples.

$$\frac{1}{d^2} = \frac{4}{3}\left(\frac{h^2+hk+k^2}{a^2}\right) + \frac{l^2}{c^2} \quad \text{..... (5.1)}$$

Where a and c represent the lattice parameters. h, k, and l are the miller indices of identified peaks while d represents the d-spacing between two lattice planes.

With the addition of metallic cations as the dopant in barium hexaferrite, a slight change in lattice parameters was observed, probably because of minute change in ionic radii of iron and metallic cations.

Table 5.1 Lattice parameters of Pure and Doped BaM

Sr. No.	**Prepared Sample**	**Lattice parameters**		**Crystallite Size**
		a=b	c	
1	$BaFe_{12-3x}O_{19}$ (Mn, Ni, Co)$_x$ where x=0	5.88	23.03	36.58nm
2	$BaFe_{12-3x}O_{19}$ (Mn, Ni, Co)$_x$ where x=0.2	5.88	23.09	39.47nm
3	$BaFe_{12-3x}O_{19}$ (Mn, Ni, Co)$_x$ where x=0.35	5.89	23.09	44.10nm
4	$BaFe_{12-3x}O_{19}$ (Mn, Ni, Co)$_x$ where x=0.5	5.89	23.09	55.18nm

5.2 Fourier Transform Infrared Spectroscopy

FTIR analysis was performed in the range of 2500 cm^{-1} to 350 cm^{-1} to understand the nature of chemical bonds present in the prepared sample. The figure shows the FTIR peaks of pure and doped barium hexaferrite. Sample for FTIR analysis was prepared by homogenous mixing of sample and potassium bromide and then the powder is converted into pellets.

It can be inferred from analyzing the peaks that the nature of chemical bonds in all the samples is the same as the peaks are almost undifferentiable. These absorption bands are attributed to the vibrations of sub-lattices present in the hexagonal structure of barium hexaferrite i.e. tetrahedral and octahedral sub-lattices.

Metal and oxygen bonds, present in the tetrahedral and octahedral sub-lattices, cause the stretching and bending vibrations resulting in the absorption bands. The position of the band for the octahedral and tetrahedral site differs slightly because of the difference in bond length of Fe-O.

v_1 and v_2 frequency bands correspond to the tetrahedral and octahedral sites in barium hexaferrite, respectively. The vibrational frequency of the tetrahedral site is higher than the octahedral site because the bond lengths in the tetrahedral site are shorter. As the dopant concentration is increased from x= 0 – 0.5, the tetrahedral vibration frequency-shifted toward a lower frequency range. This behavior can be attributed to the replacement of Fe^{+3} ions by the dopant metallic cations. As the bond length increases at the tetrahedral sites, the vibrational frequency is shifted toward the lower range.

Table 5.2 Tetrahedral (v_1) and Octahedral (v_2) Frequency Bands of Prepared Samples.

Sample	v_1 (cm^{-1})	v_2 (cm^{-1})
$BaFe_{12}O_{19}$	589.03	429.40
$BaFe_{12-3x}(Mn, Ni, Co)_{0.2}\ O_{19}$	587.10	427.36
$BaFe_{12-3x}(Mn, Ni, Co)_{0.35}\ O_{19}$	580.10	426.94
$BaFe_{12-3x}(Mn, Ni, Co)_{0.5}\ O_{19}$	579.52	427.51

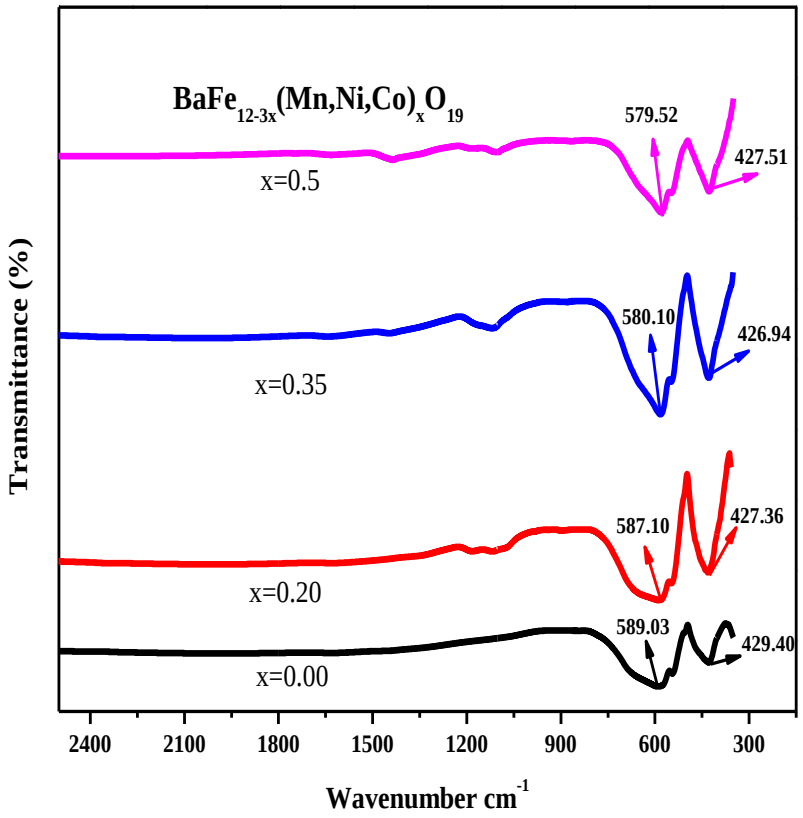

Figure 5.3: FTIR Analysis of Samples [$BaFe_{12-3x}O_{19}(Mn, Ni, Co)_x$]

5.3 Dielectric studies

The prepared sample powder was pressed into pallets using hydraulic press and then sintered at high temperature to analyze the Dielectric constant, dielectric loss, tangent loss, AC conductivity and AC impedance.

5.3.1 Dielectric Constant:

Dielectric constant is a result of polarization which can be either interfacial, dipolar electronic or ionic polarization. Dielectric constant has:

i- Real Part

ii- Imaginary Part

Real part of the dielectric constant deals with energy storage abilities of the material or polarization. Fig shows the variation of dielectric constant with frequency for each sample. There is a decreasing trend in dielectric constant with the increase of frequency for each prepared sample and it eventually become constant. This trend is attributed to the decrease in space charge polarization as the frequency rises. At higher frequencies, the dipoles are unable to line up because of sudden shift of electric field applied. At lower frequencies, the value of dielectric constant seems to be higher. The calculated value of dielectric constant for pure barium hexaferrite at 500 Hz is 2.29×10^{2}. Dielectric constant increased with increasing concentration of metallic cation dopants $BaFe_{12-3x}\ O_{19}(Mn, Ni, Co)_x$. The highest value of dielectric constant 1.45×10^{3} at 500 Hz came for x=0.5. The increasing trend of dielectric constant with increasing concentration of dopant at 500 Hz is shown in figure below:

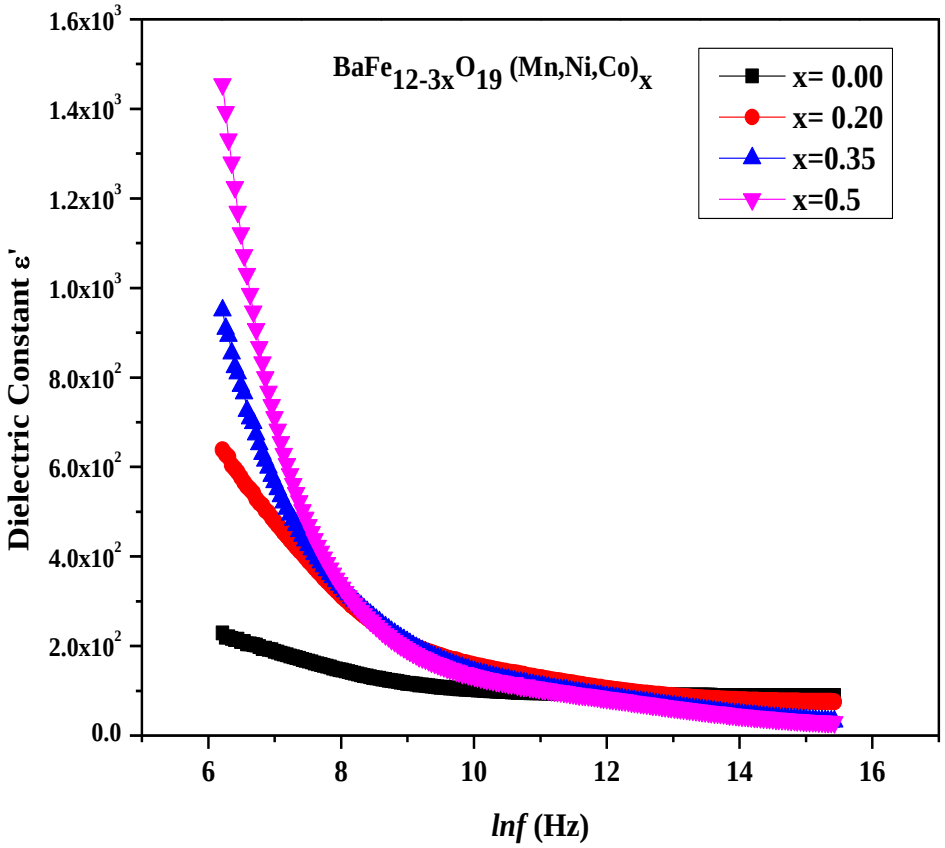

Figure 5.4: Dielectric Constant Variation with frequency for [$BaFe_{12-3x}\ O_{19}(Mn, Ni, Co)_x$]

The increase of dielectric constant values at lower frequencies can be well explained by Maxwell and Wagner model of space charge polarization [37]. According to this model, a dielectric material is divided into two parts, grains and grain boundaries. Grains are considered to be relatively conductive while grain boundaries are highly resistive. When an external field is applied, the electrons start to move toward grain boundaries. Accumulation of electrons happens at the grain boundaries because of the resistive nature of boundaries and result in the polarization of material.

Accumulation of charge carriers occur at grain boundaries when the frequency of applied field is low, causing the space charge polarization resulting in high values of dielectric constant. At higher frequencies, a slow response is shown by these charge carries which result in decrease in space charge polarization and ultimately low values of dielectric constant.

Table 5.3 Dielectric Constant values of Pure and Doped BaM.

Sample	**Dielectric Constant**
$BaFe_{12}O_{19}$	2.29×10^{2}
$BaFe_{12-3x}(Mn, Ni, Co)_{0.2}\ O_{19}$	6.38×10^{2}
$BaFe_{12-3x}(Mn, Ni, Co)_{0.35}\ O_{19}$	9.50×10^{2}
$BaFe_{12-3x}(Mn, Ni, Co)_{0.5}\ O_{19}$	1.45×10^{3}

With the addition of metallic cations, an increase in dielectric constant can be seen in the figure. Metallic cations will occupy the tetrahedral sites, forcing the Fe^{+3} ions to migrate toward the octahedral site. Hence the electron hoping between Fe^{+3} to Fe^{+2} on the octahedral site will increase resulting in enhanced polarization. Also, the difference in electronegativity value of doped metallic cations and iron is less as compared to barium hence they will donate their electrons to iron resulting in increase of charge carrier. With increased number of charge-carriers the space charge

polarization also increases so the dielectric constant will increase with high dopant concentration.

5.3.2 Dielectric Loss:

Energy dissipation can be stated in terms of dielectric loss. The trend of dielectric loss with frequency is shown below in the figure. The values of dielectric loss are decreasing with increase of frequency. With the increasing addition of dopant, the dielectric loss is seemed to increase.

At lower values of frequency, dielectric loss has higher values. Dielectric loss values start to decrease as the frequency of the applied field is increased. Also, with the increasing dopant concentration the value of dielectric loss increased from 90.8 for pure barium hexaferrite to 1790 for barium hexaferrite doped with Mn, Ni and Co where x= 0.5

The decreasing behavior of dielectric loss at higher frequencies can be explained by Koop's theory. According to this theory, polarization requires more energy in low frequency regions because of highly resistive grain boundaries. Hence energy losses are high. Whereas, resistivity of grain boundaries in high frequency region is relatively lower so the polarization of material become slight easy. Hence the dielectric losses start to decrease.

Table 5.4 Dielectric Loss values of Pure and Doped BaM.

Sample	Dielectric Loss
$BaFe_{12}O_{19}$	9.08×10^{1}
$BaFe_{12-3x}(Mn, Ni, Co)_{0.2}\ O_{19}$	5.47×10^{2}
$BaFe_{12-3x}(Mn, Ni, Co)_{0.35}\ O_{19}$	1.10×10^{3}
$BaFe_{12-3x}(Mn, Ni, Co)_{0.5}\ O_{19}$	1.79×10^{3}

With increasing dopant concentration, increase in dielectric loss can be seen in the figure. Movements of charge carriers in the alternating electric field cause the dissipation of energy and hence the dielectric loss occurs. As the doping concentration is increased, number of charge carrier moving in the alternating electric field also increase causing high dielectric losses. Therefore, dielectric loss is highest for x=0.5 concentration of dopant in barium hexaferrite.

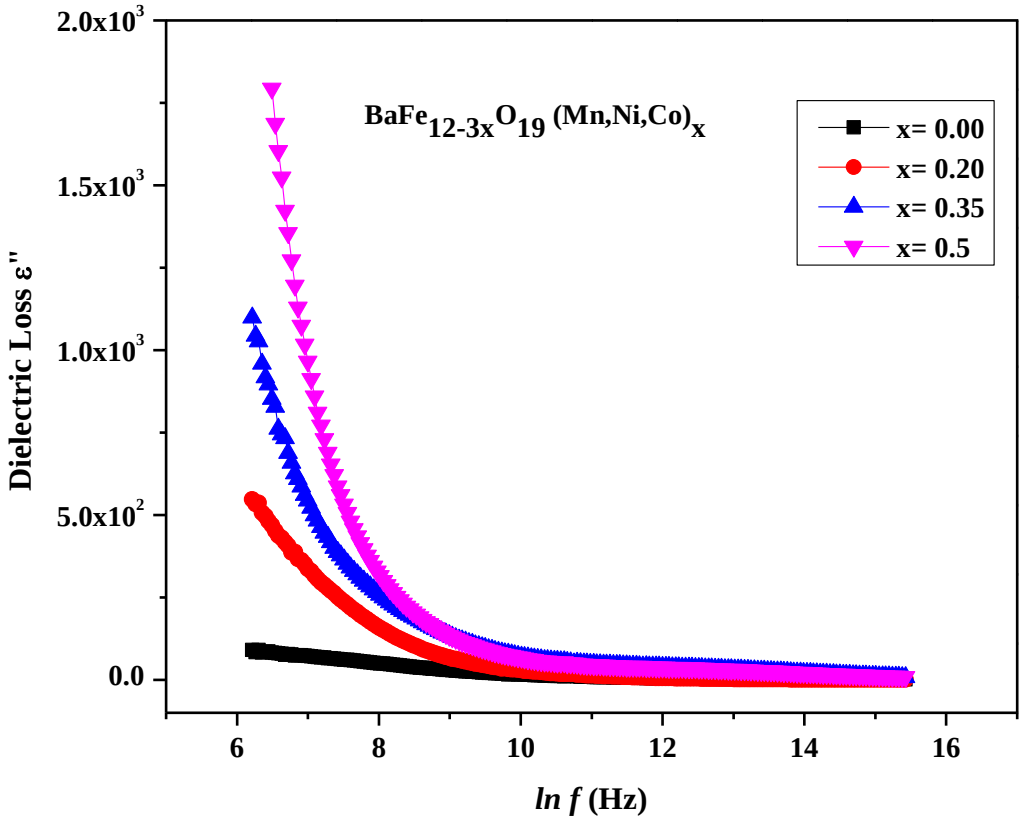

Figure 5.5: Dielectric Loss Variation with frequency for [$BaFe_{12-3x}O_{19}$(Mn, Ni, Co)x]

5.3.3 Dielectric Tangent Loss

Tangent loss is given by ratio of complex part of permittivity to real part i.e. Ɛ''/ Ɛ'. Dielectric tangent loss quantifies the relative dissipation of energy due to applied alternating electric field. Figure shows the plot of dielectric tangent loss and natural log of frequency of applied field. At low frequencies, the tangent loss is high because

the hopping of electron between Fe^{+3} and Fe^{+2} is higher whereas this hopping reduces at higher frequency resulting in decrease of dielectric tangent loss values.

Table 5.5 Dielectric Tangent Loss values of Pure and Doped BaM.

Sample	Dielectric Tangent Loss
$BaFe_{12}O_{19}$	0.39
$BaFe_{12-3x}(Mn, Ni, Co)_{0.2}\ O_{19}$	0.85
$BaFe_{12-3x}(Mn, Ni, Co)_{0.35}\ O_{19}$	1.15
$BaFe_{12-3x}(Mn, Ni, Co)_{0.5}\ O_{19}$	1.23

Also, with the increase of dopant concentration, the dielectric tangent loss is also increased. The value of tangent loss for pure barium hexaferrite is 0.396 whereas when BaM is doped with x=0.5 Mn, Ni and Co, the tangent loss value is increased to 1.79. This increase in dielectric tangent loss with concentration can be attributed to increase number of charge carriers in doped samples which require high amount of applied field energy for space charge polarization. Hence the dielectric tangent loss increases.

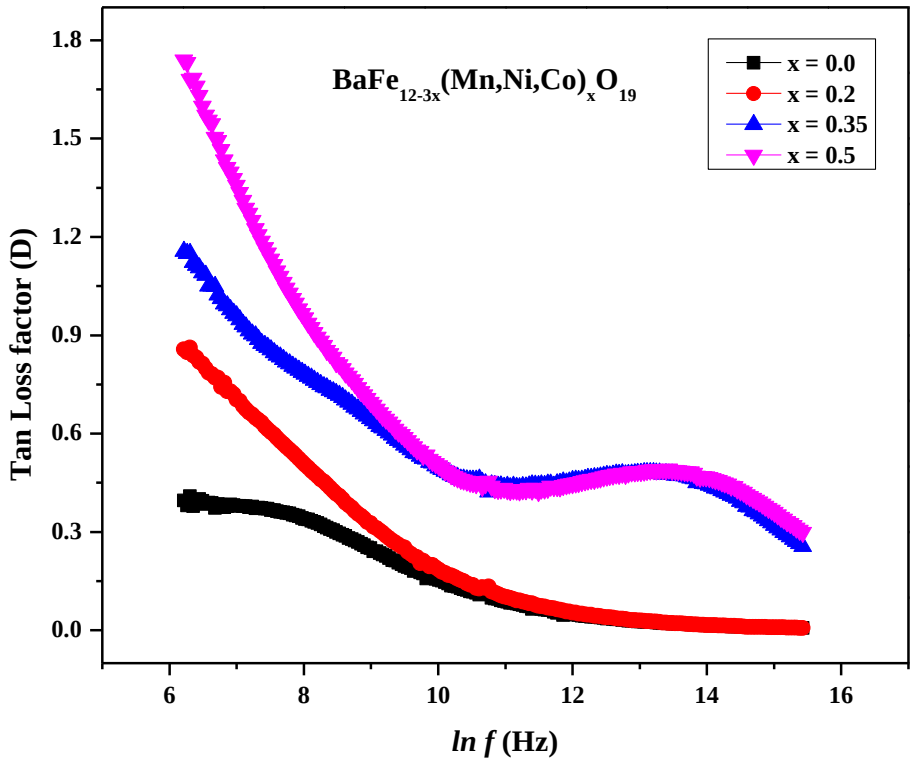

Figure 5.6: Dielectric Tangent loss Variation with frequency for[$BaFe_{12-3x}O_{19}$(Mn, Ni, Co)x]

5.4 Magnetic Measurements

Vibrating sample magnetometer was used for magnetic measurements of the pure and doped samples to study the magnetic properties. M-H loop of pure barium hexaferrite and $BaFe_{12-3x}$ (Mn, Ni, Co)$_x$$O_{19}$ at x=0.0, 0.2, 0.35, 0.5 was measured using VSM with maximum magnetic field of 15 kOe and shown in figure below.

Grain sizes of the magnetic materials have effect on the magnetic coercivity values. The magnetic hysteresis loop of all the prepared samples suggests that they are hard magnetic materials because of high coercivity values. Pure barium hexaferrite has high value of H_c because it possesses uniaxial anisotropy i.e. it has one easy axis along the c-axis. Figure also shows an increase in saturation magnetization M_s for each doping concentration from x = 0 to x = 0.5. With the increase of dopant concentration, a decrease in coercivity H_c value is observed suggesting that material became relatively

softer. Hence, for $BaFe_{12-3x}$ (Mn, Ni, Co)$_x$O$_{19}$ Hc value is 413.48 kAm^{-1} at x = 0, H=299.47 kAm^{-1} at x=0.2, H=268.11 kAm^{-1} at x= 0.35 and Hc= 274.22 kAm^{-1}.

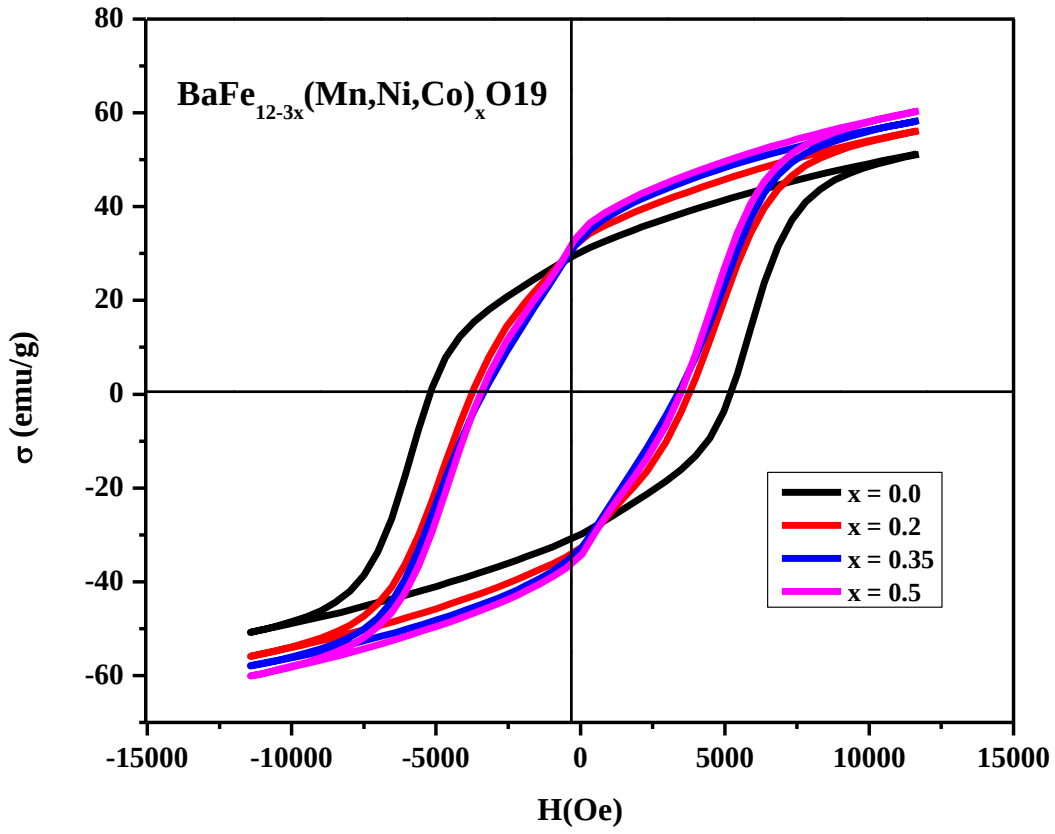

Figure 5.7: Hysteresis loop for $BaFe_{12-3x}O_{19}$(Mn, Ni, Co)$_x$ sample

Saturation magnetization of barium hexaferrite doped with various concentration of Mn, Ni and Co was increased with increasing concentration of dopant. This trend can be attributed to the substitution of Mn^{+2}, Ni^{+2} and Co^{+2} in $4f_1$ tetrahedral site. There are five interstitial sites for Fe^{+3} ion: 12k, 2a 2b, $4f_1$ and $4f_2$. 12k and 2b sites are favorable for the high level of substitution and have upward spin of electron. $4f_1$ and $4f_2$ site is suitable for low substitution level ~0.5 and have downward electron spin. If the substitution occurs at site with downward spin of electron, the saturation magnetization increases [38]

When Barium hexaferrite is doped with metallic cations, the number of unpaired electrons with upward spin at $4f_1$ site start to increase resulting in increasing of total magnetic moments. Hence, the net saturation magnetization is increased. So

Ms=51.2emu/g for pure barium hexaferrite, Ms=56.1emu/g for x=0.2, Ms=58.2emu/g for x=0.35 and Ms=60.3emu/g for x=0.5.

Similarly, the value of remanence magnetization Mr can also be calculated using VSM result. For pure barium hexaferrite, the Mr= 24.0emu/g. There is an increase in remanence magnetization with increasing dopant concentration. So, Mr=32.6 at x=0.2, Mr=33.0 at x=0.35 and Mr= 34.2 at x=0.5.

Table 5.6 Values Saturation Magnetization, Remanence and Coercivity of Pure and Doped BaM

Sample	**M_s (emu/g)**	**M_r (emu/g)**	**H_c (kAm^{-1})**
$BaFe_{12}O_{19}$	51.2	24.0	413.48
$BaFe_{12-3x}(Mn, Ni, Co)_{0.2}\ O_{19}$	56.1	32.6	299.47
$BaFe_{12-3x}(Mn, Ni, Co)_{0.35}\ O_{19}$	58.2	33.0	268.11
$BaFe_{12-3x}(Mn, Ni, Co)_{0.5}\ O_{19}$	60.0	34.2	274.22

Conclusion

There has been a great work done in hexagonal ferrites during the last ten years for a number of applications. Particularly they find their use in electronic industry for wireless communications such as mobile phones at MW/GHz frequencies, in the absorption of electromagnetic wave, stealth technologies, and radar radiation absorber materials and also as composite materials. Due to their expanded use, hexaferrites gain importance as magnetic material being produced at commercial scale. Barium based M-type hexaferrites ($BaFe_{12}O_{19}$) is one of such materials that is currently used in these applications.

In the present work, barium hexaferrite doped with cobalt, manganese and nickel is synthesized using auto-combustion sol gel method. The metal nitrates were dissolved in deionized water to make an aqueous solution and then used to prepare the samples with desired composition. Characterization of prepared samples was performed using x-ray diffraction analysis and Fourier transforms infrared spectroscopy. Moreover, dielectric properties of the pure and doped barium hexaferrite were measured using impedance analyzer. Magnetic properties are also being studied using vibrating sample magnetometer.

The formation of $BaFe_{12-3x}(Mn, Ni, Co)_x O_{19}$ was confirmed by the x-ray diffraction analysis. The band position of the vibration frequencies were studies using FTIR. Dielectric properties were studies at room temperature. The dielectric constant seemed to increase from 2.25×10^2 at x = 0 to 1.4×10^3 at x = 0.5. The dielectric loss increased from 90.8 at x = 0 to 1790 at x = 0.5.

Vibrating sample magnetometer (VSM) was used to analyze the magnetic properties of the prepared samples. It has been observed that the saturation magnetization is increasing with the increase of dopant concentration. Ms was 51.2 emu/g for pure barium hexaferrite and it increased to 60.3 emu/g at x = 0.5. Magnetic Coercivity studies of the pure and doped sample revealed a decrease in the value of coercivity with increasing dopant concentration.

These materials are very good for use in electrical application, charge storing devices, superconductors and EMI shielding.

Future Work

The composite with different polymers can be made in order to study different properties including mechanical, electrical and optical properties.

The prepared samples can render very useful in various industrial applications. Properties can be varied and improved by changing percentage of ingredients.

The electrical properties of samples $Ba_{1-x}Sr_xFe_{12-3x}$ (Mn, Ni, Co)$_xO_{19}$ can be studied by varying x to make a comparative study.

References

[1] M. R. Rehman, Scripta Materialia, 57 (2019) 1093-96.

[2] M. &. A. M. H. M. Rostami, J. Ceramics International 45 (2019) 7606-7613.

[3] E. a. A. V. Spain, (2014).

[4] V. &. M. V. Marghussian, J. Ceramics International 45 (2015) 4360-4367.

[5] S. &. A. E. SHAMEBO, "studies on structural, electric, dielectric and magnetic properties of nickel-based ferrite materials".

[6] A. A. Birajdar, J. Physics Research International, (2012).

[7] V. G. Harris, J. IEEE Transactions on Magnetics 48 (2011) 1075-1104.

[8] P. V. C. F. &. B. P. Coutinho, J. Solid State Communications 252 (2017) 59-63.

[9] N. P. Solanki, J. Nanotechnology and Nanomaterials (2016) 305-325.

[10] A. N. A. Y. M. S.H. MAHMOOD1*, J. Solid State Phenomena 232 (2014) 65-92.

[11] P. S. R. J. G. Kajal K. Mallick ∗, Journal of the European Ceramic Society 27 (2007) 2045-52.

[12] A. K. a. S. S. Paramdeep Kaura, J. Materials Today: Proceedings 14 (2019) 426-434.

[13] M. Sugimoto, Journal of the American Ceramic Society 82 (1999) 269-280.

[14] b. E. G. S. H. Y.-J. W. D. L. K.S. Martirosyana, J. Materials Science and Engineering 176 (2011) 8-13.

[15] S. S. R. P. L. K. P. a. Sunil Kumara), J. Materials transactions 48 (2018) 465-470.

[16] M. R. M. H. M. Radwan ∗, J. magnetism and magnetic Materials 337 (2013) 65-69.

[17] Y. n. Y. Daming Chen, J. magnetism and magnetic Materials 337 (2013) 65-69.

[18] n. H. H. A. H. Sözeria, J. Ceramics International 40 (2014) 8645-8657.

[19] S. R. Pratap Behera, J. Solid State Sciences 89 (2019) 139-149.

[20] H. M. M. B. G. H. &. A. R. S. Hossein Nikmanesh, J. Ceramics International 42 (2016) 14342-14349.

[21] S. Y. M. &. M. A. Mesdaghi, J. Materials Chemistry and Physics 236 (2019) 121786.

[22] R. S. M. M. &. N. H. Alam, J. Materials Research Bulletin 73 (2016) 261-267.

[23] V. C. S. S. E. M. M. L. K. R. H. &. M. S. S. Chavan, J. Magnetism and Magnetic Materials 398 (2016) 32-37.

[24] K. K. S. P. &. G. R. J. Mallick, J. Magnetism and Magnetic Materials 312 (2007) 418-429.

[25] M. G. &. S. S. C. Shalini, J. AIP Conference Proceedings 1728 (2016) 2044.

[26] M. R. M. A. M. T. A. K. F. A. K. A. A. M. S. &. S. M. Waqar, J. Applied Physics 124 (2018) 286.

[27] V. B. M. P. S. V. S. G. &. C. E. Galstyan, J.Chemosensors 6 (2018) 16.

[28] S. E. W. D. J. S. S. M. M. L. &. L. S. Shirsath, J. Handbook of sol-gel science and technology (2018) 695-735.

[29] R. B. D. P. S. U. &. S. B. G. Sharma, J. Recent Research in Science and Technology, (2012).

[30] R. S. S. F. C. M. K. R. M. D. M. A. S. &. S. F. S. M. Melo, J. Magnetism and Magnetic Materials 381 (2015) 109-115.

[31] L. L. X. H. X. X. Z. T. D. J. Z. F. .. &. H. C. Yuan, J. ACS nano 6 (2012) 656-661.

[32] W. M. Doyle, J. Process Control Qual 2 (1992) 11-41.

[33] T. &. A. C. Nicolet, in J. Thermo Nicolet Corporation (2001).

[34] J. S. N. &. J. R. Balavijayalakshmi, J. Magnetism and Magnetic Materials 385 (2015) 302-7.

[35] T. S. Tripathi, (2011).

[36] B. &. V. B. Kirupakar, J. pharmaceutics and Drug Analysis 4 (2016) 227-233.

[37] J. C. Maxwell, A treatise on electricity and magnetism, (1873).

[38] S. Farooq, PhD diss., Quaid-i-Azam University Islamabad, (2010).

[40] S. H. Kareem, (2016).

[41] H. M. Khan, (2016).

[42] L. A. Vaughan, (2011).